THE UNIVERSITY OF OKLAHOMA

GRADUATE COLLEGE

THE TEMPERATURE DEPENDENCE OF LIGHT SCATTERING BY IMPERFECTIONS IN SOME ALKALI HALIDE CRYSTALS

A DISSERTATION

SUBMITTED TO THE GRADUATE FACULTY

in partial fulfillment of the requirements for the

degree of

DOCTOR OF PHILOSOPHY

BY

MARVIN LEE BREIG

Norman, Oklahoma

1963

THE TEMPERATURE DEPENDENCE OF LIGHT SCATTERING BY IMPERFECTIONS IN SOME ALKALI HALIDE CRYSTALS

APPROVED BY

DISSERTATION COMMITTEE

ACKNOWLEDGEMENTS

I wish to express my extreme thanks to Professor Colin A. Plint not only for suggesting the problem, but also for the many helpful discussions which led to its completion.

My thanks also go to Dr. William A. Sibley of the Oak Ridge National Laboratory for photometric analysis done in this thesis.

I wish also to express my gratitude to my wife for her help in the completion of this work.

M.L.B.

TABLE OF CONTENTS

LIST OF TABLES

LIST OF ILLUSTRATIONS

THE TEMPERATURE DEPENDENCE OF LIGHT SCATTERINGS BY IMPERFECTIONS IN SOME ALKALI HALIDE CRYSTALS

CHAPTER I

INTRODUCTION

Ionic crystals, such as the alkali halides, constitute a very convenient class for the investigation of crystal imperfections by optical techniques. In particular, the relative ease of production of pure materials of good crystallographic quality and the fairly thorough knowledge of the binding forces, diffusion mechanisms, dislocation arrangements, color centers, etc. in these crystals make them desirable not only for experimental work but also in the field of theoretical physics.

For purposes of discussion, one may consider a real, or imperfect, crystal and an ideal, or perfect, crystal.

An ideal crystal (1) may be thought of as a regular repetition in space of a fundamental or unit cell. The atoms are arranged in a lattice having three fundamental translation vectors $\vec{a}$, $\vec{b}$, $\vec{c}$ with the property that, viewed along them, the atomic arrangement looks the same from any point on the lattice. Then, the operation of translation $\vec{r} = n\vec{a} + l\vec{b} + m\vec{c}$, where n, l, m are integers, leads to a final configuration in the crystal that is identical to the initial one. The atoms in an ideal crystal are confined to regular lattice sites, and each

lattice site has its required quota. No vacancies or other imperfections are present, and the crystal extends to infinity. Ionic conduction, diffusion, and many other physical properties that characterize a material would not be present since these properties are dependent upon the imperfections present. The ideal crystal would be of theoretical value only since these crystals obviously do not occur in nature. It is at once apparent that the type and number of imperfections present in a real crystal are of utmost importance when one wishes to understand many of the physical properties of solid matter.

The crystals of alkali halides, being of cubic structure, are perhaps the simplest type to investigate. At the same time it is hoped that the results obtained for this type crystal may be extended to predict results for more complicated crystal structures. The common types of imperfection (2) in ionic crystals are:

I. vacancy (vacant lattice site): this can be either positive or negative

II. interstitial: an ion moved from a regular lattice site to a position somewhere between regular sites

The energy of formation of an interstitial ion in alkali halides is much greater than the energy of formation of a vacancy, thus interstitials are of minor importance for natural defect properties of these materials. Interstitials are formed by the passage of particles through the crystals; however, such interstitials are not in thermal equilibrium with the lattice.

III. color center: negative ion vacancy that has captured an electron; positive ion vacancy that has captured a hole; etc.

An imperfection of this type absorbs light of a particular frequency and the crystal appears colored.

IV. divalent impurity: foreign ion of valence + 2 replaces an ion of valence + 1 in the lattice

V. vacancy-impurity complex: divalent positive ion impurity and a neighboring positive ion vacancy.

The aforementioned imperfections are usually considered "point imperfections" because they are localized in a small region. Of the five point imperfections listed I, IV, and V are the most common in alkali halide crystals. However, although the imperfection itself is localized to a small region, the lattice around the imperfection will be distorted so that the "point imperfection" effectively covers several lattice sites. A localized collection of point imperfections is termed a "bad region," and these bad regions are spread throughout the crystal.

Some of the physical properties of a crystal depend on the size and number of these bad regions. For example, a measure of the ionic conductivity in ionic crystals provides a direct method of determining not only the concentration but also the mobility of vacancies. Other experiments (3) tend to show that extensive assemblies of point imperfections, other than the random distribution of vacancies or bad regions, must also be present in ionic crystals. If one attempts to measure the yield strength by applying external force to the crystal, one finds the experimental yield strength to be from 10 to 100 times smaller than the value arrived at from calculations made for an ideal crystal (4). In order to explain the mechanical weakness observed, one is forced to conclude that sources are present that can cause one part of the crystal to slip past a neighboring part at very low applied stress. These extended sources are called dislocations.

A dislocation is an extended bad region, most probably much larger in one direction than in the other, in which case it is termed a

dislocation line. The type of dislocations considered here may be conveniently grouped into two categories, the edge and the screw.

An edge dislocation is formed when an extra half plane of atoms is forced into the crystal lattice:

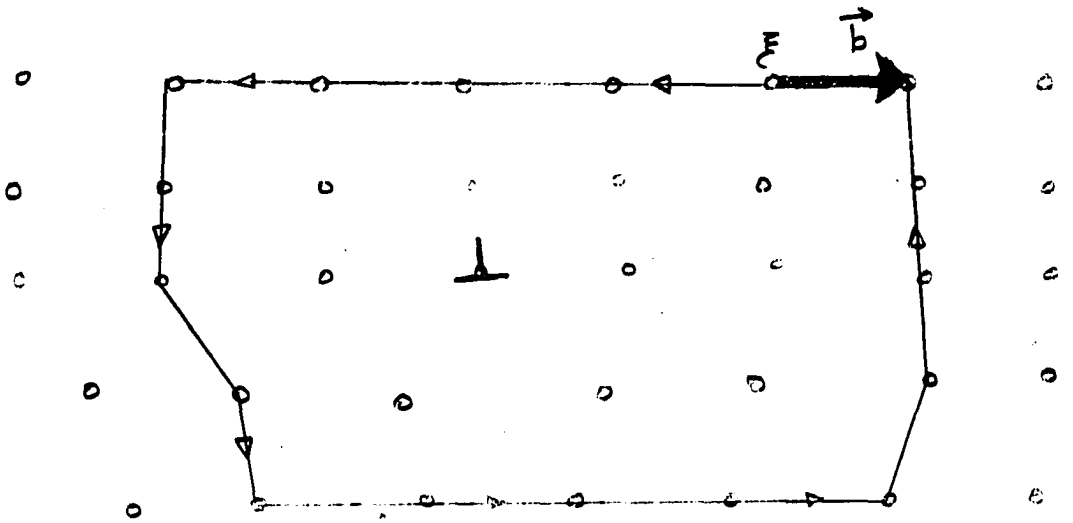

Fig. 1.--Edge Dislocation

The region immediately surrounding the edge of the extra half plane is known as the dislocation line. This may be seen from figure 1. The "strength" of an edge dislocation is measured in terms of a "Burgers' vector." It is defined as follows: if one starts at a point ξ far removed from the dislocation line and attempts to traverse the dislocated region by counting the same number of atoms in each direction along the edges of a square with the dislocation at the center, one finds that because of the extra half plane the figure does not close. A vector connecting the starting point with the end point is called the Burgers' vector. Its magnitude can be a few atomic distances. The Burgers' vector $\vec{b}$ must always connect one equilibrium position with another. The smallest amount of slip occurs when $|\vec{b}|$ is one lattice spacing.

A dislocation with this vector is called a unit dislocation, or one of unit strength. On the other hand, dislocations of strengths greater than unity are unstable because they have high strain energies and can decompose into two or more dislocations of lower strengths, thereby lowering the strain energy.

Frank (5) has emphasized that the Burgers' vector is the most invariant characteristic of a dislocation line; it is the same for all parts of the line and remains the same when the dislocation moves. In the case of the edge dislocation, the Burgers' vector is perpendicular to the dislocation line.

One describes a screw dislocation in much the same way as an edge dislocation:

Fig. 2.--Screw Dislocation

To visualize a screw dislocation, take a cylindrical region and cut a slice such as is shown in figure 2(a) above. Then lift one side of the cut upward and force the other side downward. Figure 2(b) results. The resulting dislocation line is along the axis of the cylinder. If one traverses the bad region in a manner similar to the method used for the edge dislocation, one finds that the Burgers' vector in this case is

parallel to the dislocation line. As in the case of the edge dislocation, the strongly distorted lattice extends for a few atomic distances in each direction away from the dislocation line.

Slip occurs when one part of the crystal slides as a unit across a neighboring part. If the surface on which slip occurs is planar, it is called a slip plane. At any stage during consecutive slipping we could always, in principle, draw a line in the slip plane around the boundary of each slipped region. This boundary is called a slip dislocation. A slip dislocation in a crystal is highly mobile in the sense that, when it moves on a slipped surface, the resistance that the lattice offers to its motion is small and may be overcome by a small applied stress, several orders of magnitude smaller than the shear modulus. If an edge dislocation moves along a slip plane, the half plane of atoms remains unchanged and the motion is termed conservative. If the dislocation moves in a direction other than on a slip plane, the extra half plane of atoms must be transported. This is called non-conservative motion. Since a screw dislocation has no extra half plane, there is no non-conservative motion and the dislocation is free to move on any cylindrical surface having the slip direction for its axis. It should therefore have a higher mobility than the edge dislocation.

Because of the localized dilation of the lattice associated with the edge dislocation, vacancies and impurities can be attracted to the dislocation line and form an atmosphere of defects around the line. In addition, when vacancies condense on the dislocation line and take the place of ions, jogs may be formed and the dislocation line will appear to have an excess electrostatic charge. More will be said about

the subject of charged dislocation lines in a later chapter. Because of its nature, a screw dislocation must be jog free and also has zero dilation. There is little tendency to form vacancy clouds around this type of dislocation.

Measurements of diffusion of radioactive tracer elements (10) along dislocation boundaries indicate that diffusion is much more rapid along the boundaries than in the rest of the crystal. This implies that there is a considerable vacancy concentration in the region around a dislocation.

Methods of Studying Crystals

I. Conductivity (6). As mentioned earlier, ionic conductivity in ionic crystals provides a direct method of measuring the mobility and concentration of vacancies. In this case one applies a steady electric field across the crystal and the positive ion vacancies and negative ion vacancies move due to the effect of the field. Neutral vacancy pairs could not be detected by this method.

II. Decoration of dislocations (7). A hole is cut in the crystal and a small amount of sodium, potassium, etc. is placed inside. The crystal is then heated to within a few degrees of the melting point. The cation diffuses throughout the crystal, moving most easily along strains such as dislocations. Small globules of the cation metal are precipitated along the diffusion paths and render the paths visible under moderate magnification. This method tells one nothing about the dislocation network before the decoration treatment and one must be content with the high temperature dislocation array or strains set up during the cooling. For KCl and NaCl under these conditions, the (111) and (100) planes seem to be preferred for networks.

III. Etching (8). When a crystal surface has been chemically etched, deep pits are formed which are visible under the microscope. It is believed that the flat bottomed etch-pits are due to precipitates present and the pyramid type etch-pits are due to dislocations. The shape of the pits at the surface gives information about the direction of the dislocation line. The number of dislocations per square centimeter extending through the surface can be measured by this method. It is evident that these etch pits are associated with defects of some kind in the crystal since:

A. The concentration of etch pits is independent of the time and temperature of the etching.

B. They are arranged in patterns typical for dislocations.

C. When a surface is chemically polished and then re-etched, the etch pits appear in the same places indicating that the defects are extended along lines.

IV. Light scattering (9). The methods of etching and decoration of disloaction lines are very informative, however they tend to alter the crystal in that in all probability new imperfections are introduced into the crystal by the method of measurement. The method of measuring the intensity of light scattered by a crystal and relating this scattered intensity to the concentration and orientation of dislocation networks has proved to be a powerful tool for the investigation of imperfections in transparent crystals without changing the status quo of the crystal. The method used will be discussed briefly in a later chapter.

Since this is a statistical method, one must sacrifice individuality for average effects. By this method one can calculate average

number of dislocations, average or effective lengths, and preferred orientations.

For an ideal crystal described earlier, there would be no scattering. As Bhagavantam (10) points out, for light scattered from any volume element in an ideal crystal, one can always find a similar element such that the phase of the two disturbances is 180° apart and the net result is zero. This is not true for an actual crystal. When the size of the scattering particles is much less than the wave length of the light, the intensity of the scattered light obeys Rayleigh's λ^{-4} law. When the size of the scattering particles approaches the wave length of the light used, deviations from Rayleigh's law occur which are easily noticeable. From measurements of the angular dependence of the scattering power, it is possible to determine the orientation of the scattering centers. The drawback to this method is the realization that precipitates would also scatter light in a manner analogous to the dislocations, and one must therefore be careful in interpreting experimental results.

The intensity of the scattered light in many good optical quality crystals is some ten times larger than thermal scattering. This increased intensity cannot in general be due to a uniform distribution of point imperfections. However, it agrees quite well with the idea of bad regions within the crystal which are characterized by an anomolous concentration of point imperfections and the accompanying strained condition in the crystal lattice.

From early measurements of the wave length dependence of the scattering power in NaCl and KCl, Theimer, Plint, and Sibley (11) deduced a characteristic length of 1000A and interpreted this to be the

average diameter of the bad regions. From extensive orientation and angular dependence measurements on KCl (12) they concluded that the scattering centers were not randomly distributed in space but prefer certain crystal-lographic directions and tend to form 2 and 3 dimensional networks having straight sections 30,000-50,000A in length and parallel to $\langle 100 \rangle$ directions. These same authors found a pronounced maximum in the temperature dependence of the scattering power for NaCl which could be explained tentatively in terms of charged dislocations. Thus it appears that at least some of the bad regions are charged dislocations surrounded by vacancy and impurity clouds.

Taurel and Humphreys-Owen (12) studied quartz imperfections by the method of light scattering. They were primarily interested in the variation of scattered light flux with temperature, wave length, and time after change of temperature. Anomalous scattered flux was found to be divisible into two distinct fractions. The first fraction was highly anisotropic and orientation-sensitive and is consistent with the idea of "needles" lying parallel to the C axis. This fraction reacts at a different rate to change of temperature, depending on whether the temperature is raised or lowered, and was called the "slow structure." Initially the scattered flux drops as the temperature is increased. During all cooling stages the scattering flux decreased and appeared to be a linear function of temperature. After a sufficient number of heating and cooling cycles the heating curves and the cooling curve merged into a single straight line whose slope was greater than that predicted by thermal scattering by the factor two. The authors interpret this result in terms of impurity atoms which form atmospheres near edge dislocations. When the temperature is lowered there is a drift toward the atmospheres, and when the temperature

is raised there is a faster diffusion away. The second fraction, termed the fast structure, is not readily explained in terms of defects but it was suggested by the authors that defects could be indirectly responsible for the modification by interacting with the lattice vibrations. The fast structure contribution is proportional to the absolute temperature and appears to be reversible.

CHAPTER II

STATEMENT OF THE PROBLEM

Past work, in which imperfections in alkali halide crystals have been studied by light scattering techniques, has introduced many new problems that need to be answered if this phase of solid state physics is to continue to grow.

In this thesis the following problems will be considered:

(1) Measurement of equilibrium temperature dependence of the Rayleigh scattering in NaCl, KCl, and KBr from approximately 90° K to temperatures within 50 degrees of the melting point. This set of experiments was intended to extend the earlier investigation of Plint, Theimer, and Sibley (11) in order to provide more information on the possible relation between light scattering and charged dislocations.

(2) Investigation of any time changes in the scattering after change of temperature. This experiment was intended to determine whether the structure observed by Taurel and Humphreys-Owen for quartz was in fact also present in ionic crystals of the alkali halide type (13).

(3) Investigation of quench effects on the scattering power. This portion, when compared to part (1) should answer the question as to whether the high temperature quench work done by Sibley (26) actually is a measure of the high temperature configuration.

(4) Etch pit analysis of the crystals. This was needed merely

as an aid in the corroboration of data.

(5) Impurity analysis of the crystals. This analysis was vital in view of the fact that Koehler (23) considers the impurity content to be a controlling factor in determining saturation of the dislocation core.

The following work was done in the order listed above.

CHAPTER III

THEORY OF LIGHT SCATTERING BY DISLOCATIONS

To study the phenomena of light scattering by dislocations, we first formulate the existing theory of what is already known about the subject. We consider first point imperfections and "work up" to the more complicated dislocation line, and thence to networks of dislocations.

As was mentioned earlier, a perfect crystal will not scatter light since if we consider any arbitrary scattering center, we can in general find a second scattering unit positioned in such a manner that the scattered light from these two points will arive at the point of observation exactly 180 degrees out of phase and hence cancel. Consider a point imperfection in a real crystal. The electric field of the incident radiation induces a dipole in the scattering unit. This oscillating dipole has the same frequency as the incident radiation and will emit radiation of its own. In an ideal crystal the resultant intensity is zero for reasons cited above, but in a real crystal where thermal fluctuations in density or microscopic static inhomogeneities occur, the resultant intensity is not zero and a residual scattering is observed.

For the purpose of calculation, consider the Hertz (14) Vector $\vec{Z}$ which combines the vector potential $\vec{A}$ and the scalar potential ϕ and at the same time implies the Lorentz condition. It is defined by the equations:

$$\vec{A} = \frac{1}{c^2}\frac{\partial \vec{Z}}{\partial t} \qquad \phi = -\vec{\nabla}\cdot\vec{Z} \tag{1}$$

where

$$\vec{C} = \vec{\nabla} \times \vec{Z}$$

$$\vec{B} = \frac{1}{c^2}\frac{\partial \vec{C}}{\partial t} \tag{2}$$

$$\vec{E} = \vec{\nabla} \times \vec{C}$$

from electromagnetic theory.

Next consider plane polarized light incident on the scattering unit which is located at the origin of a coordinate system. The light is coming from the negative x direction with electric field vector in + z direction.

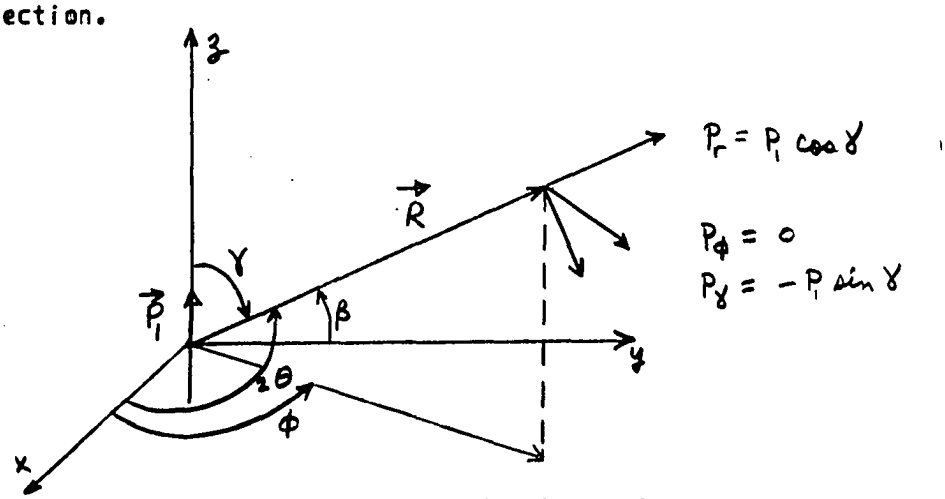

We next define the charge and current densities from a single vector function $p(X',t)$ such that:

$$\vec{\nabla}\cdot\vec{p} = -\rho_{\text{true}}$$

$$\frac{\partial \vec{P}}{\partial t} = \vec{J}_{\text{true}}$$

where ρ_{true} is the real charge density, and $\vec{J}_{\text{true}}$ is the real current density. $\vec{P}$ is known as the polarization vector. By combining the definitions of $\vec{p}$ and $\vec{Z}$, we find that if the Hertz Vector obeys

the inhomogeneous wave equation with $\vec{p}$ as source, then the ordinary potentials ϕ and $\vec{A}$ obey their respective wave equations with ρ and $\vec{J}$ as source. That is, we have:

$$\Box^2 \vec{Z} = \nabla^2 \vec{Z} - \frac{1}{c^2} \frac{\partial^2 \vec{Z}}{\partial t^2} = -\frac{\vec{p}}{\epsilon_0} \tag{3}$$

The solution of this equation is given by:

$$Z(X_\alpha) = \frac{1}{4\pi\epsilon_0} \int \frac{[\vec{p}\,(X'_\alpha)]}{r(X_\alpha, X'_\alpha)} \, d\tau' \tag{4}$$

and the Fourier components are:

$$Z_\omega = \frac{1}{4\pi\epsilon_0} \int \frac{\vec{p}_\omega\,(X'_\alpha)\, e^{ikr}}{r\,(X_\alpha, X'_\alpha)} \, d\tau' \tag{5}$$

The primed coordinates refer to the source, and the unprimed coordinates refer to the point of observation. The $[\ldots]$ means that evaluation is made at the time when the radiation was emitted rather than at the time it was observed. When the condition that the wave length is long in comparison to the size of source is fulfilled, and also the condition for dipolar field, we get

$$\vec{Z}_\omega\,(X_\alpha) = \frac{e^{ikR}}{4\pi\epsilon_0 R} \int \vec{p}_\omega\,(X'_\alpha)\, d\tau' = \frac{e^{ikR}}{4\pi\epsilon_0 R} \vec{p}_1 \tag{6}$$

which is the Hertz potential for a dipole field. The components of the Hertz potential in spherical coordinates are:

$$Z_R = \frac{e^{ikR}}{4\pi\epsilon_0 R} \, p_1 \cos\gamma \tag{7}$$

$$Z_\phi = 0 \tag{8}$$

$$Z_\gamma = \frac{-e^{ikR}}{4\pi\epsilon_0 R} \, p_1 \sin\gamma \tag{9}$$

By using the above expressions (equation 2) for $\vec{E}$ and $\vec{B}$ we find:

$$E_\gamma = -\frac{k^2 p_1 \sin\gamma \; e^{ikR}}{4\pi \epsilon_0 R} \; ; \; H_\phi = -\omega \frac{k p_1 \sin\gamma \; e^{ikR}}{4\pi R} \qquad (10)$$

To calculate the energy radiated along $\vec{R}$ direction, one calculates the time average of the Poynting Vector:

$$I = \tfrac{1}{2} \overline{\mathrm{Re} \left| E \times H^* \right|} = \frac{\omega k^3 p_1^2}{32\pi^2 \epsilon_0 R^2} \sin^2\gamma \qquad (11)$$

or, since $\omega/c = k$ and $p_1 = \alpha E_0$,

$$I = \frac{\omega^4 \alpha^2 E_0^2}{32 c^4 \pi^2 R^2 \epsilon_0} \sin^2\gamma \qquad (12)$$

where α is the average polarizability. Then:

$$P = \frac{I}{I_0} = \frac{\omega^4 \alpha^2}{32 c^4 \pi^2 R^2 \epsilon_0} \sin^2\gamma \qquad (13)$$

is the scattering power. If we consider the more general case of unpolarized light incident in the + x direction inducing a dipole also in y direction of value $\vec{p}_1$:

$$P + \frac{\omega^4 \alpha^2}{32\pi^2 c^4 R^2 \epsilon_0} (\sin^2\gamma + \sin^2\beta) \qquad (14)$$

But $\cos^2\gamma + \cos^2\beta + \cos^2 2\theta = 1$, therefore:

$$P = \frac{\omega^4 \alpha^2}{32\pi^2 c^4 R^2 \epsilon_0} (1 + \cos^2 2\theta) \qquad (15)$$

The factor $(1 + \cos^2 2\theta)$ is known as the Thomson scattering factor.

If we next consider a system of point defects and sum their contributions to the total scattering power observed at point $\vec{R}$ we must remember that radiation from each point defect has traveled a

different distance and, hence, one must take into account the possible interference effect because of phase differences. Also, the strength of each induced dipole will depend on the material around the scattering unit, and hence the polarizability will not be a constant but will depend on the position in the crystal.

We define the effective polarizability as the difference between the polarizability of an ideal crystal and the polarizability of a defect and write the effective polarizability associated with the nth defect as α_{n^*} .

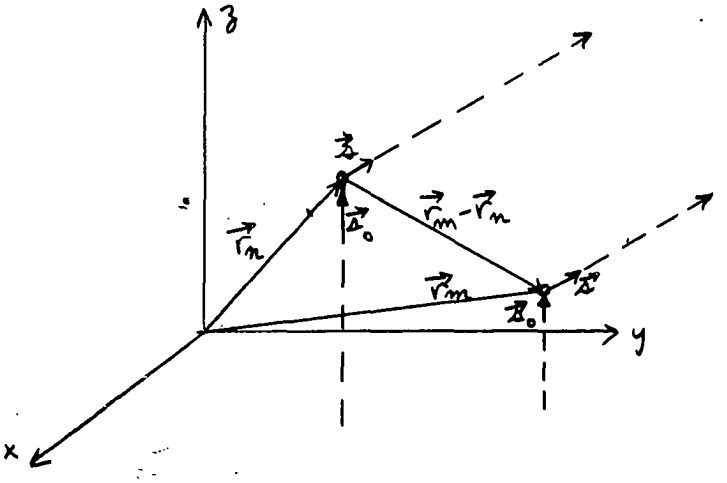

In the above figure $\vec{s}_0$ and $\vec{s}$ are unit vectors in the direction of the incident and scattered light respectively. The path difference between the light scattered from the nth defect and the mth defect is $(\vec{r}_m - \vec{r}_n) \cdot (\vec{s} - \vec{s}_0)$. The phase difference is then $\frac{2\pi}{\lambda}(\vec{r}_m - \vec{r}_n) \cdot (\vec{s} - \vec{s}_0)$, which may be reduced to $\frac{2\pi}{\lambda}\vec{r}_m \cdot \vec{S}$ by a proper choice of origin. Here we define $\vec{S} = \vec{s} - \vec{s}_0$. Hence for a distribution of point defects, the scattering power is:

$$P = \frac{\omega^4 (1 + \cos^2 2\theta)}{32\pi^2 c^4 R^2 \epsilon_0} \left| \sum_m \alpha_{m^*} e^{i\frac{2\pi}{\lambda}\vec{r}_m \cdot \vec{S}} \right|^2 \quad (16)$$

If we now define a new vector $\vec{\mu} = \frac{2\pi}{\lambda}\vec{S}$, the scattering power takes

the form:

$$P = \sigma(\theta\lambda) \left| \sum_m \alpha_m^* e^{i \vec{\mu} \cdot \vec{r}_m} \right|^2 \qquad (17)$$

where $\sigma(\theta\lambda) \equiv \frac{\omega^4 (1 + \cos^2 2\theta)}{32\pi^2 c^4 R^2 \epsilon_0}$. By inspection, one can see that $\vec{\mu}$ lies in the scattering plane and bisects the angle between $\vec{s}_0$ and $\vec{s}$:

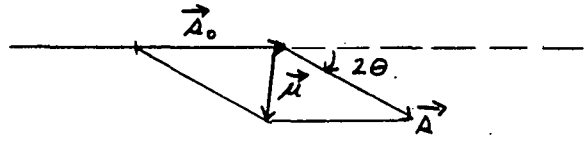

If there is only one type of defect present, the effective polarizability may be replaced by an "average effective polarizability" $\overline{\alpha^*}$ and taken outside the summation. If one also defines a distribution function $\rho(xyz)$ such that $\rho(xyz)d\tau$ represents the average number of defects in the volume $d\tau$, one may replace the sum by an integral:

$$P = \sigma(\theta\lambda) \overline{\alpha^*}^2 \left| \int_\tau \rho(xyz) e^{i \vec{\mu} \cdot \vec{r}} \, d\tau \right|^2 \qquad (18)$$

Equation 18 may then be put in the following form:

$$\frac{\sqrt{P(\theta\lambda)}}{\sqrt{\sigma(\theta\lambda)}\,\overline{\alpha^*}} = + \iiint_0^R \rho(r) e^{i \vec{\mu} \cdot \vec{r}} r^2 d\cos\chi \, dr d\phi \qquad (19)$$

Call $p(\mu) \equiv \sqrt{P(\theta\lambda)}$, and after integration over the angular part, one obtains:

$$\frac{p(\mu)}{\sqrt{\sigma(\theta\lambda)}\,\overline{\alpha^*}} = \frac{4\pi}{\mu} \int_0^R r \, \rho(r) \sin \mu r \, dr \qquad (20)$$

Now $P(\theta,\lambda) \longrightarrow 0$ with increasing R , hence the limit of integration

may be extended to infinity if the volume $>> r^{*3}$, where r^* is the radius of the region containing the defects. Next perform a Fourier inversion to obtain $\rho(r)$.

$$\rho(r) = \frac{2}{\pi r} \int_0^\infty \frac{\mu p(\mu) \sin \mu r \, d\mu}{4\pi \sqrt{\sigma(\theta\lambda)} \alpha^*} \tag{21}$$

Remembering that λ is a function of μ we may replace $\sigma(\theta\lambda)$ by $\sigma(\theta)\mu^4$, since $\vec{\mu} = \frac{2\pi}{\lambda} \vec{s}$. Hence we obtain:

$$\rho(r) = \frac{1}{2\pi^2 r \alpha^* \sqrt{\sigma(\theta)}} \int_0^\infty p(\mu) \frac{\sin \mu r}{\mu} d\mu \tag{22}$$

If one measures $p(\mu)$ from light scattering techniques, it is then possible to determine $\rho(r)$, the distribution function. From $\rho(r)$ and the point of deviation from Rayleigh's law, one can calculate an effective radius and an effective length of the bad region. Plint, Theimer, and Sibley (11) and also Theimer, Plint, and Sibley (12) find 1000A to be the average effective radius of bad regions in ionic crystals; and 50,000A their most probable length.

These extended bad regions are identified with dislocations; and since their length is much greater than their width, they are probably very closely associated with the dislocation lines.

From the preceding discussion it appears that we may describe a dislocation line as a row of interstitial atoms or vacancies with a cylindrically strained lattice surrounding it. For purposes of evaluation of the scattering by a cylindrical bad region, consider the two coordinate systems (xyz) and (x'y'z'), where $\vec{r} = r(xyz)$ and $\vec{\mu} = \mu(x'y'z')$.

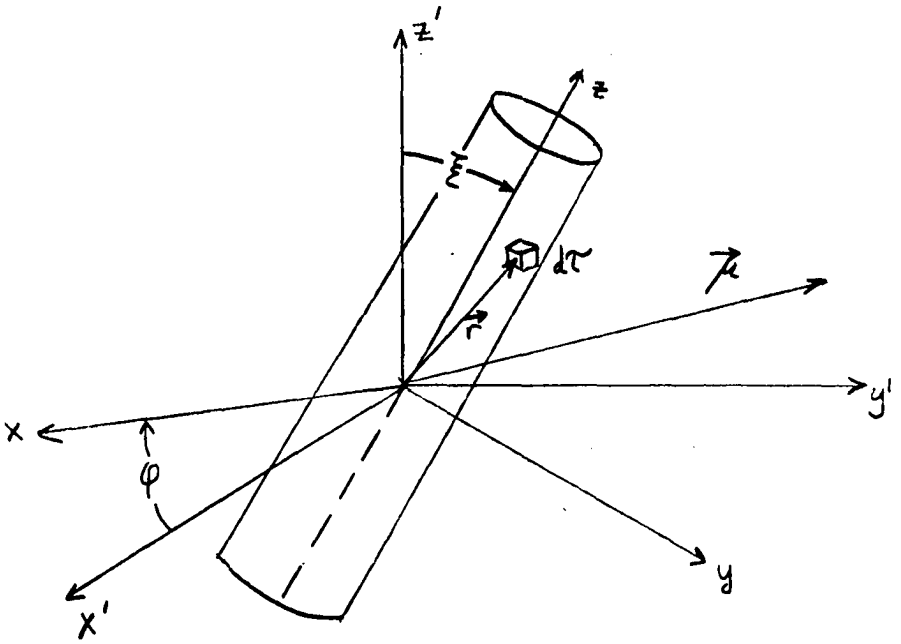

Cylinderical coordinates of $d\tau$ are $(r\cos\chi, r\sin\chi, z)$. $x'y'z'$ is a triad fixed in space from which $\vec{\mu}$ is measured. xyz is a triad fixed in the dislocation line with z measured along the axis of the dislocation. At this point it is convenient to express in terms of the unprimed coordinates in order to evaluate $\vec{\mu}\cdot\vec{r}$:

$$\vec{\mu}\cdot\vec{r} = Ar\cos\chi - Br\sin\chi + Cz \qquad (23)$$

where

$$\begin{aligned} A &= \mu\cos\vartheta\ \cos\varphi + \mu\sin\vartheta\ \sin\varphi \\ B &= \mu\cos\vartheta\ \cos\xi\ \sin\varphi - \mu\sin\vartheta\cos\xi\cos\varphi \\ C &= \mu\cos\vartheta\ \sin\xi\ \sin\varphi - \mu\cos\vartheta\ \sin\xi\cos\varphi \end{aligned} \qquad (24)$$

Substituting this value into the scattering power formula gives:

$$P = \sigma(\theta)\frac{2}{\alpha^*}\left|\int_\tau r\ \rho(r)e^{-i(Ar\cos\chi - Br\sin\chi + Cz)}dr\,dz\,d\chi\right|^2 \qquad (25)$$

Since $\rho(r)$ does not depend on z, one may integrate over z:

$$P = \sigma(\theta)\overline{\alpha^*}^2\left[\frac{\sin^2\frac{CZ^*}{2}}{(\frac{CZ^*}{2})^2}\right]\left|\int_0^{\infty}\int_0^{2\pi} r\rho(r)e^{-i[Ar\cos\chi - Br\sin\chi]}drd\chi\right|^2 \quad (26)$$

This is as far as a computation of this type can be carried unless one knows more about the form of $\rho(r)$. Lester (15) evaluates this integral for several types of density distribution functions.

For a system of N rod-like dislocations among which there is no constant phase relation, the scattering power may be found by adding the individual contributions of all the dislocations.

One can calculate the scattering power for any type of regular network of dislocations by using the appropriate distribution function for the network and proper phase summation over the system (16, 17).

Some conclusions (9, 11, 12) drawn from the foregoing work are:

I. Wave length dependence experiments reveal the existence of a characteristic dimension of order 1000A in KCl.

II. In Harshaw crystals of KCl and KBr the scattering centers are cylindrical rods oriented along $\langle 100 \rangle$ crystallographic axes, which are about 50,000A long and 200-500A in diameter.

III. Etch-pit analysis of the crystals indicated that all of the dislocations etched were perpendicular to the (100) cleavage plane.

IV. Diametrically opposed peaks in scattering power versus angle were observed, which moved through an angle 2ϕ when the crystal was rotated through angle ϕ. This is the type of scattering pattern one would expect from cross-shaped networks of dislocations. Upon comparing the positions of the peaks with the directions of the crystal axes, it was determined that the scattering bad regions were oriented

preferentially in $\langle 100 \rangle$ directions and thus are probably closely associated with dislocation lines in the same directions. This result is in agreement with those of other investigators who found that the $\{110\}$ planes are preferred slip planes in the alkali halides.

Charged Dislocations

If the free energy of formation of positive ion vacancies and negative ion vacancies in ionic crystals is not the same, and if, as Lohovec (18) has pointed out, the vacancies can be formed only at the crystal surface, we obtain a more complicated state of affairs than was originally estimated in calculating the number of Schottky defects present in an ionic crystal.

If the energy of formation of positive ion vacancies is lower than for negative ion vacancies, then positive ion vacancies will be more easily formed than negative ion vacancies. Hence, when the temperature is raised from absolute zero an excess of positive ion vacancies is emitted from the surface into the crystal leaving the surface with a net positive charge. This resulting space charge encourages the emission of negative ion vacancies. In equilibrium the bulk of the crystal must be electrically neutral, but there is a positive charge layer on the surface and an equal and opposite negative charge cloud within the crystal. Hence a potential difference exists between the surface and the interior of the crystal.

Now a dislocation may be considered a free surface within the crystal, and hence is surrounded by a charged layer of this type. In this sense we speak of the dislocation as being surrounded by a charge cloud, the line itself being oppositely charged. This charge cloud

also contains divalent impurities which enter the lattice in a substitutional manner. If the cloud is immobile a finite force will be needed to separate it from the dislocation, and the crystal will then possess a yield stress below which plastic flow will not occur. If, as seems possible, the extent and magnitude of the charge cloud is temperature dependent, several interesting phenomena should occur. For example, at low temperatures, where the charge cloud around the dislocation is certainly immobile, some of the impurities may precipitate out in a new phase and hence reduce the impurity concentration which takes part in ion cloud formation. Therefore, the yield strength should be a complicated function of temperature, having a minimum at the points where the smallest amount of force is needed to separate the charge cloud from the dislocation. This effect should occur when the charge on the dislocation vanishes and then the yield strength is determined by the unual mechanical forces associated with dislocation motion and generation. The temperature at which the charge vanishes is called an isoelectric temperature.

Eshelby et.al. (19) have measured the yield strength of NaCl as a function of temperature and report a minimum in yield stress at about 300° K. They also point out that this temperature, where the dislocation should have zero net charge, must also be intimately related to the concentration of divalent impurities present. Hence, from a knowledge of the isoelectric points and also the impurity concentration, it should be possible to determine the energy of formation of the vacancies.

Metag (20) has obtained data showing that the yield stress and the tensile stress for fracture both depend sensitively on the divalent impurity concentration and on the annealing given the samples of NaCl before testing. The NaCl sample used by Metag contained $PbCl_2$ as impurity

in a concentration of 10^{-4}. He records a minimum of yield stress at 400° C, which implies that the energy of formation for positive ion vacancies in NaCl is $E_F^+ = 0.534$ eV., if one uses the analysis of Koehler (23) discussed later. Since the formation energy for a +, - vacancy pair is 2.02ev., it appears that the energy of formation of a positive ion vacancy is indeed less than that of a negative ion vacancy.

Burgsmuller (21) measured the tensile strength of rock salt of higher purity and observed a minimum at 40° C. However he fails to mention the exact impurity content of the crystals used in his investigation.

Sproull (22) applied strong electrostatic fields to LiF crystals that had been bent and reported that the bend moved from 0.1A to 6.0A. This motion was analyzed in terms of charged dislocations, and he concluded that the dislocation core had a charge of order 10^{-4} to 10^{-3} esu/cm. and presumably arose from the inequality of formation energies of positive and negative ion vacancies.

Plint, Theimer, and Sibley (12) extended the theory of Lehovec and Eshelby et. al. to light scattering phenomena and estimated the probable charge on a dislocation line to be $\leq \frac{1}{2}e$ per ion spacing. This represents a charge per unit length of dislocation to be -8.6×10^{-3} esu/cm.

Koehler, Langreth, and von Turkovich (23) have extended the work of Eshelby et. al. and show that the charge clouds around dislocations are important for the mechanical properties of ionic crystals. This paper appears to be the most complete to date and hence will be discussed in some detail.

As we mentioned at the beginning of this section, if the energy of formation of positive ion vacancies is less than the energy of formation of negative ion vacancies and if these vacancies can only be formed at a free surface, then the surface will acquire a positive charge and an equal and opposite charge in the form of a space charge will extend from the surface a short distance. A dislocation may be considered a free surface and hence will acquire a positive charge, while a charge cloud of opposite sign will surround it.

There are two conditions that must be satisfied if equilibrium is to be attained. First, the charge distribution must satisfy Poisson's equation. Secondly, the free energy of the system must be a minimum. The concentrations of positive and negative ion vacancies are then given by the Boltzman distribution:

$$n_+ = N \exp\left[- (E_F^+ - ev)/kT)\right] \qquad (27)$$

$$n_- = N \exp\left[- (E_F^- + ev)/kT \right] \qquad (28)$$

where v(r) is the electrostatic potential at a point inside the crystal and N is the number of positive ion sites/unit volume. The divalent impurities should also be distributed according to a Boltzman distribution if they can diffuse at the temperature under consideration:

$$n_i = \gamma N \exp\left[-ev/kT \right] \qquad (29)$$

Poisson's equation may then be written:

$$\nabla^2 v = \frac{-4\pi\rho}{\epsilon} = \frac{-4\pi}{\epsilon} e (n_i + n_- - n_+) \qquad (30)$$

If one next makes use of a dimensionless potential p(r) defined as follows:

$$p(r) \equiv e\, v\,(r)/\, k\, T \quad , \qquad (31)$$

then the divalent impurity concentration may be written:

$$n_i = \gamma N \exp (- e v / k T) \tag{32}$$

$$\frac{n_i}{N} = \gamma \exp (- p (R)) = C$$

where $r = R$ at a point midway between dislocations. c represents the average divalent impurity concentration at a point far from the dislocation line. At this point the crystal must be neutral, i.e. $n_i + n_- - n_+ = 0$. Hence at $r = R$:

$$C + \exp\left\{ - \left[E_F^+/kT + p(R) \right] \right\} - \exp\left\{ - \left[E_F^-/kT - p(R) \right] \right\} = 0 \tag{33}$$

Solving equation (33) for $e\,p(R)$ one arrives at the expression:

$$ep(R) = e^{E_F^+/kT} \left\{ \frac{c}{2} + \sqrt{\frac{c^2}{4} + \exp \left[- (E_F^+ + E_F^-)/kT \right]} \right\} \tag{34}$$

In most cases of interest, the second term under the square root is ten times smaller than the first, hence one can set

$$ep(R) = C e^{E_F^+/kT} \tag{35}$$

If we next substitute (27), (28), (31), (32), and (35) into (30), one arrives at Poisson's equation in the convenient form

$$\nabla^2 z = \frac{8\pi N e^2 C}{\epsilon kT} \sinh z \tag{36}$$

where $z(r) = p(r) - p(R)$. (37)

Equation (36) is the working equation for the study of charged dislocations. This equation was solved by Eshelby et. al. for the condition $ev(r)/kT \ll 1$ which has the solution

$$p(r) = A K_0 (Kr) \tag{38}$$

where K_0 is the modified Bessel function and $\kappa^2 = \frac{8\pi e^2 Nc}{\epsilon kT}$. By subtle reasoning Eshelby et. al. (19) show that $1/\kappa$ is very nearly the radius of the charge cloud surrounding the dislocation. From equation (38) the charge on the dislocation is then given by

$$\sigma = \frac{\epsilon AkT}{2e} \sinh \frac{eV(R)}{kT} \tag{39}$$

Koehler et. al. have shown that the situation considered by Eshelby is not the most common case, and in fact $ev/kT \gg 1$ for most cases of interest. A very important point discussed by Koehler is the establishment of boundary conditions for equation (36) in the neighborhood of the dislocation line. At the point $r = R$ midway between two dislocations, the potential $z(r) = 0$. Also at this point

$$\left(\frac{dz}{dr}\right) = 0. \tag{40}$$

This means that the electric field is zero midway between dislocations, and arises because each dislocation comprises an electrically neutral system. Koehler also shows by minimizing the free energy that the variation in free energy can be zero only if the potential at the dislocation core vanishes. This result is very important since it implies that a point on the dislocation core is equivalent to a point outside the crystal as was assumed by Plint, Theimer, and Sibley (11).

Case I--Saturated Core

The impurity concentration at the point r is:

$$c_i = \gamma\, e^{-p(r)} = c^2 \exp\left(E_F^+/kT\right) e^{-p(r)} \tag{41}$$

for core saturation $c_i = 1$. Therefore, since under this condition the

impurity term dominates the charge density term, $\rho \simeq e\, n_i \simeq e\, N$, and Poisson's equation may be written

$$\nabla^2 p = -\frac{4\pi N e^2}{\epsilon kT} \tag{42}$$

for the saturated core. The solution associated with zero core potential in the saturated region is

$$p = b \ln\left(\frac{r}{a}\right) - \frac{\pi N e^2}{\epsilon kT}(r^2 - a^2) \tag{43}$$

where a is the radius of the core, and b is a constant. Table I shows the various saturation temperatures of NaCl for different impurity concentrations as given by Koehler et. al.

TABLE I

C	T_s^0 K.
10^{-3}	554° K.
10^{-4}	416
10^{-5}	333
10^{-6}	273

The temperature at which the divalent impurity ion concentration at the core drops below saturation, for NaCl ($E_F^+ = 0.66$ ev).

By taking the normal derivative of equation (43) at the dislocation core ($r = a$) and using Gauss Theorem, one obtains an expression for the charge per unit length on the dislocation line:

$$q = -\frac{1}{2}\frac{\epsilon bkT}{e} + \pi N e a^2 \tag{44}$$

For $C = 10^{-5}$, $T = 300°$ K. Koehler finds the charge q per unit length of dislocation in NaCl to be 0.127 esu/cm. or -7.43 electronic charges/ionic length, which is an exceedingly high value.

Outside the saturation region, the type of solution used depends on whether $|z|$ is large or small. Koehler first divides the space surrounding a dislocation in two regions. The first region is the area immediately surrounding the core. In this region $|z| > 1$, $z < 1$, and Poisson's equation becomes

$$\nabla^2 z = \frac{d^2z}{ds^2} + \frac{1}{s}\frac{dz}{ds} = \frac{-1}{2} e^{-z} \tag{45}$$

where $s = \kappa r$. An acceptable solution in this region is:

$$e^{-z} = \frac{H}{s^2 \sinh^2\left[\frac{\sqrt{H}}{2} \ln \frac{s}{s_0}\right]} \tag{46}$$

where H is a constant.

The next region is the small $|z|$ region. The solution for this region is the Eshelby type solution:

$$z = -A K_0 (\kappa r) \tag{47}$$

Koehler next proceeds to match the solutions and derivatives across the two boundaries. From these equations the constant b in equation (44) can be determined.

Case II--The Core Is Not Saturated

If the core is not saturated one proceeds as before except that now the solutions and derivatives for large $|z|$ are matched to those for small $|z|$. For example, from Table I it may be seen that at

$C = 10^{-5}$ and $T = 500°$ K the core is no longer saturated. For this case Koehler's equations predict a charge per unit length of -1.05×10^{-3} esu/cm. or -6.12×10^{-2} electronic charges per ionic length for NaCl, which is a very reasonable value and is of the same order of magnitude as the charge determined by Sproull (22) in deformation experiments.

Results of light scattering experiments with ionic crystals indicate that at least some of the imperfections are dislocations, surrounded by vacancy and impurity clouds. Hence changes in the scattering power could conceivably be due in part to changes in the vacancy and impurity cloud surrounding the dislocation. At saturation of the dislocation core, the core would have a large charge per unit length and a dense impurity-vacancy cloud associated with it. Thus the scattering from the saturated dislocation would be relatively intense. As the temperature is raised in the direction away from saturation the charge cloud should get smaller and the scattering weaker. Similarly, if the temperature is lowered below the saturation temperature precipitation of impurity ions may occur and again the scattering should change. Effects of these types will be discussed later.

CHAPTER IV

EXPERIMENTAL PROCEDURE

In the scattering experiments of Theimer, Plint, and Sibley (12) at room temperature, the crystal was immersed in benzene, which has the same index of refraction, in order to minimize the effects of light scattered by the surface of the crystal. For low or high temperatures, however, it is difficult to find a liquid with the proper index of refraction that will neither freeze at the low temperatures nor evaporate at the high temperatures. Therefore, since the surface scattering is considerably larger than the internal scattering, some other method is needed to reduce this effect. This aim was accomplished by use of a cross-shaped crystal placed in a blackened box of the same general shape. This arrangement prevented light scattered from one crystal face from being reflected at crystal surfaces and eventually passing through the system of slits and into the camera.

Figures 3 and 4 show the low temperature scattering system including the mercury lamp, system of lenses and slits, and scattering box. The scattering box is a modification of an earlier one used by Plint, Theimer, and Sibley (11). Thermocouples were placed above and below the crystal in order to detect any temperature gradient in the crystal that could lead to thermal strains. Heater coils were placed beside the crystal to control temperature, and containers of liquid nitrogen were placed

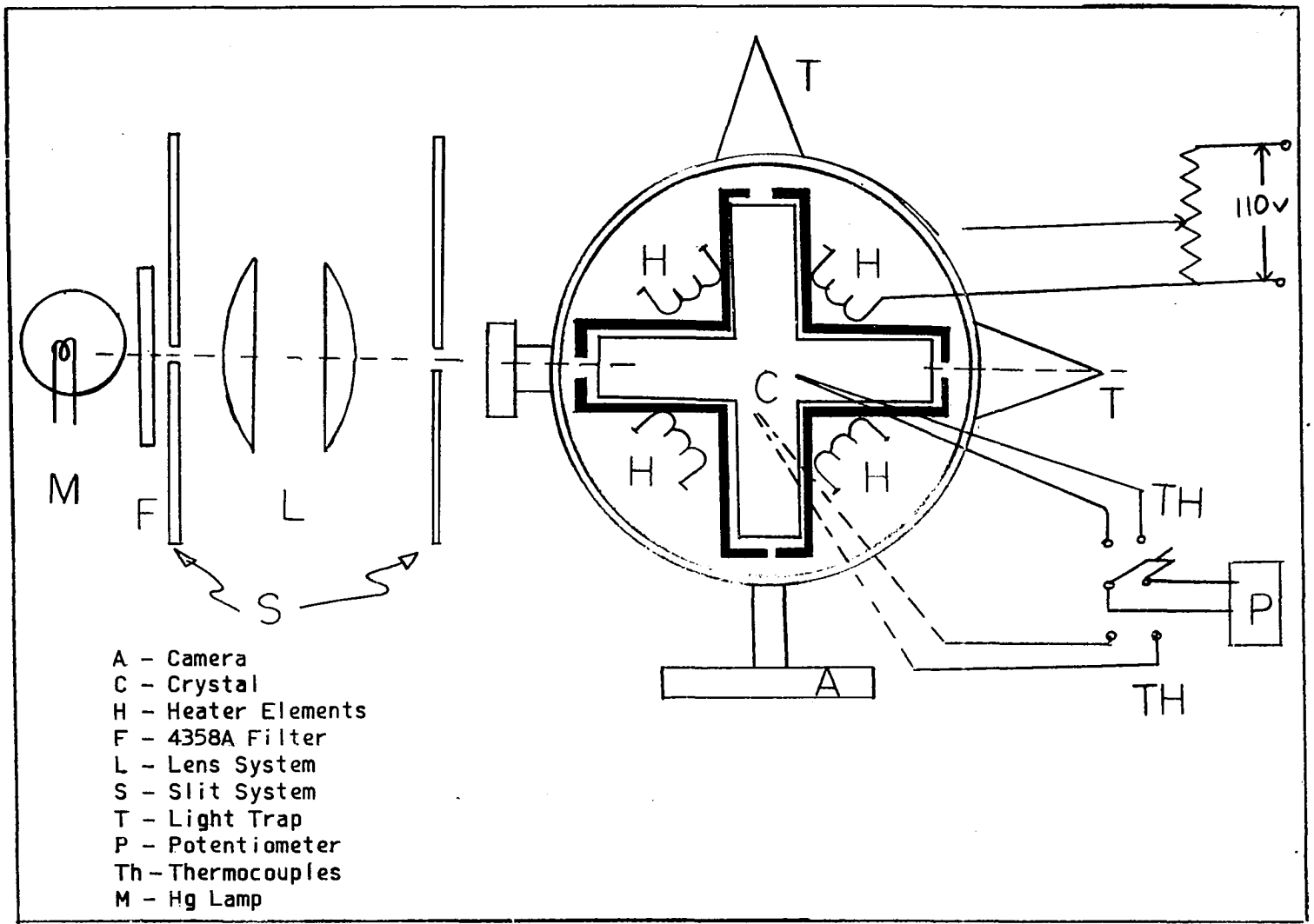

Top View

Fig. 3.--Low Temperature Scattering Box

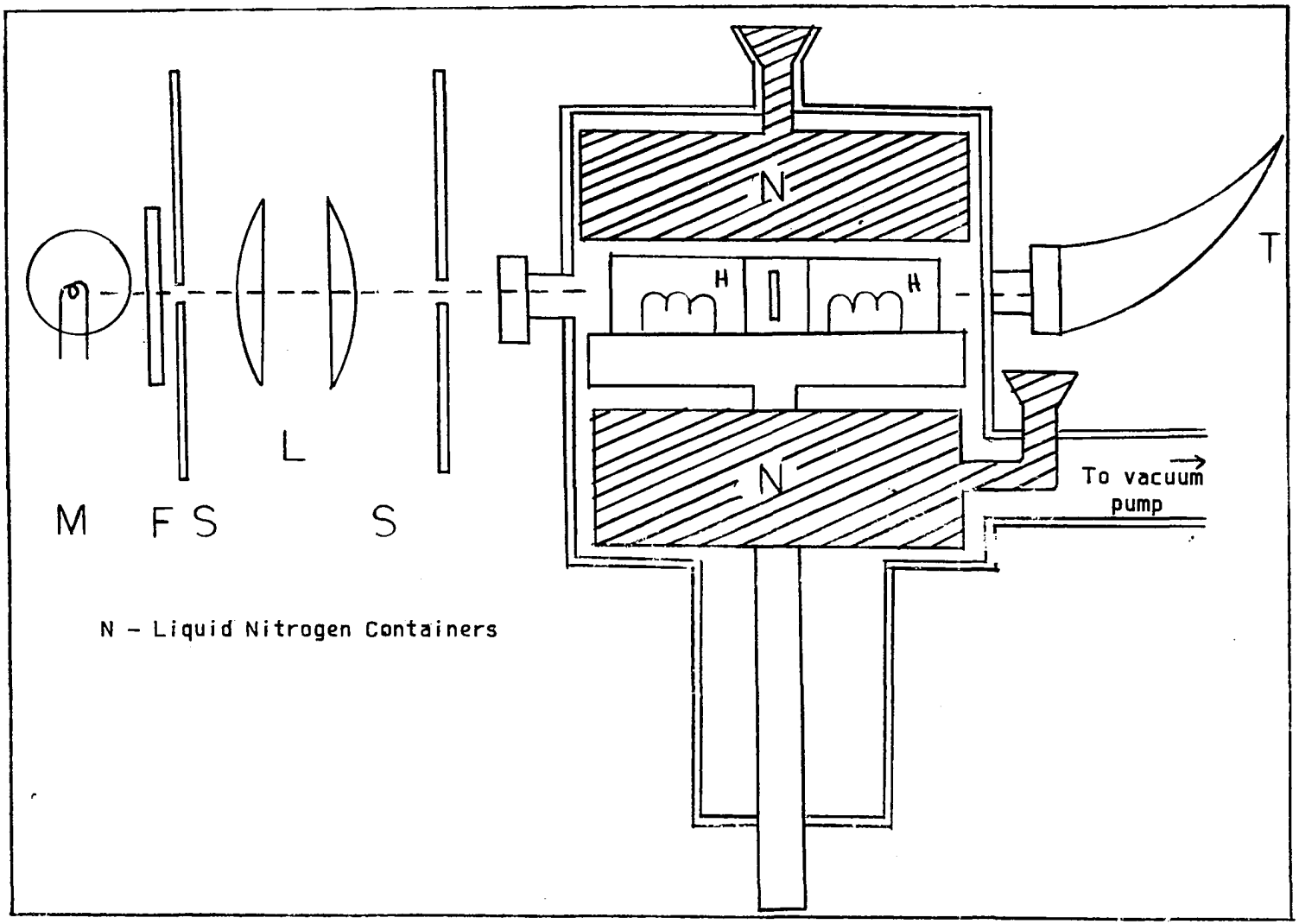

Side View

Fig. 4.—Low Temperature Scattering Box

above and below the crystal for cooling purposes. A Dewar vessel containing liquid nitrogen was also placed in contact with the lower part of the scattering box to help cool the crystal by conduction. The scattering box was covered with a layer of asbestos that served as heat insulation. A vacuum was maintained in the apparatus by an oil diffusion pump as a heat insulator, and also backed by a rotary pump. Light traps were used to prevent the direct beam from being reflected back into the scattering box. The camera was a small rectangular box capable of holding only one strip of film at a time, and this strip having dimensions of 1 cm. by 10 cm. On the front of the camera a seven step density filter could be placed when needed for intensity calibration of the film.

The light beam was well collimated and rectangular in cross section with dimensions of 1 mm. by 3.5 mm., and no change could be detected in the size of the beam in traversing the crystal.

To avoid any interpretation of source fluctuations as a change in scattering power, the source itself was observed for time intervals corresponding to those needed for the time change experiments, which amounted to about ten hours in some cases.

The blue light from mercury ($\lambda = 4358A$) was used for the entire work dealing with light scattering. It was therefore desirable to know if the observed effects were wave length dependent. We were especially interested in knowing if the peaks in scattering power were changed to higher or lower temperatures if the wave length of the incident radiation was changed. For this purpose the temperature range in the neighborhood of the peak was investigated with mercury green light ($\lambda = 5460A$) so that any change could be detected. Also to check for any change in isotropy of scattering units with temperature, experiments were run with

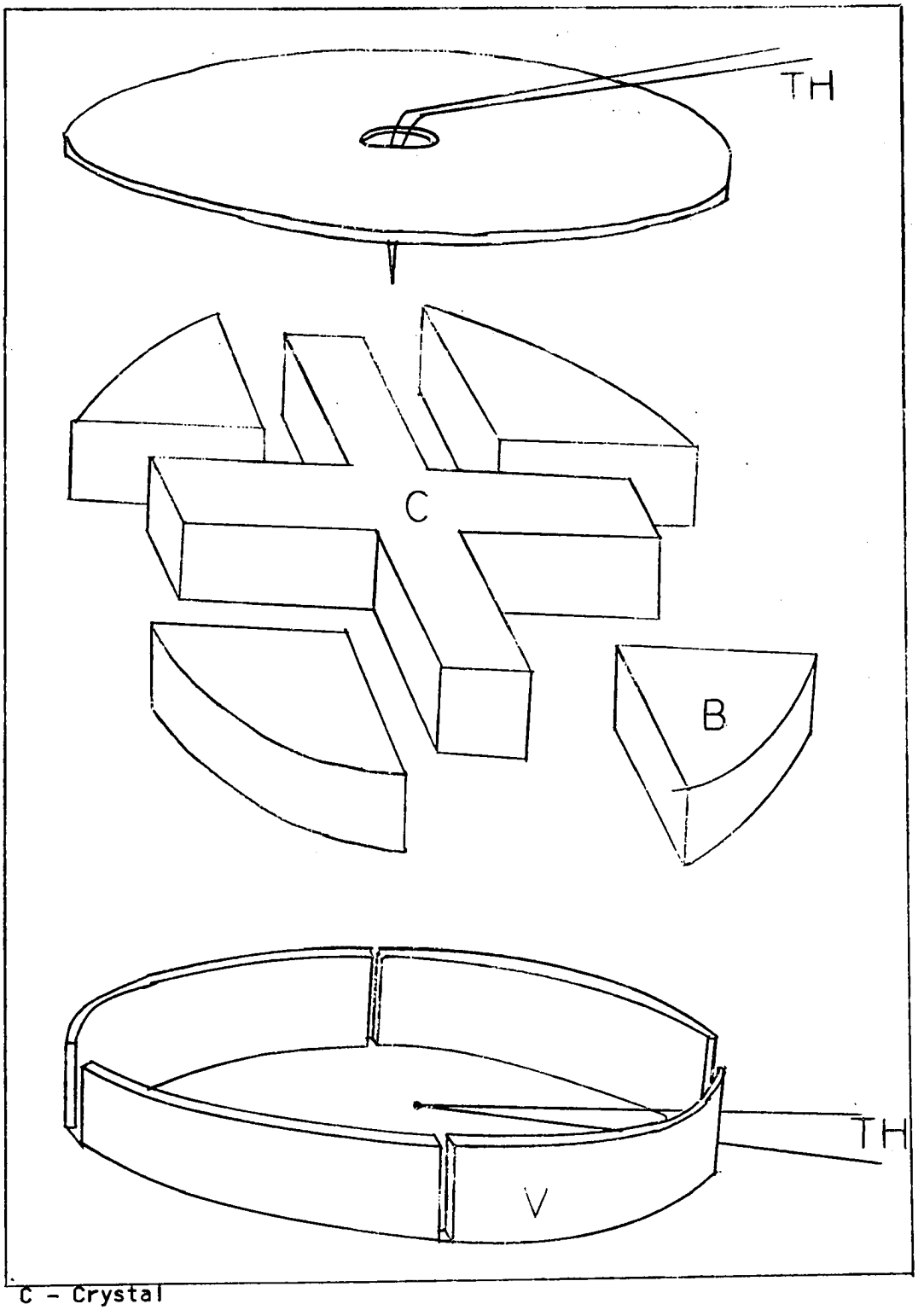

C - Crystal
H - Heater
B - Foamsil
V - Vycor boat

Fig. 5.--Interior of High Temperature Box

horizontal filters placed between the crystal and the film.

For the high temperature experiments, a different apparatus was designed since the liquid nitrogen containers on the low temperature scattering box were no longer needed, and in their place better heat insulation was desirable. The high temperature scattering box had the same general shape as that of the low temperature box. It was designed, however, to withstand temperatures up to 1000° C. which meant that a few special precautions were needed. The corrosive effect of the alkali halides on many metals at high temperatures also limited the type of material that could be used to construct the box. Vycor and quartz glass were used extensively for interior parts, and stainless steel was used for the major exterior parts. A layer of Sil-o-cel two inches thick was placed around the scattering box to cut down heat loss. The vacuum pump and oil diffusion pump were no longer needed.

Two heaters capable of dissipating 1000 watts combined power were placed above and below the crystal. The heaters had separate controls to facilitate temperature stabilization. The crystal itself was placed in a small cylindrical Vycor box 2 cm. in height and of diameter only slightly smaller than that of the scattering box. The interior of this box was made cross shaped by means of small opaque wedges of Foamsil that were placed between the arms of the crystal. By this method we effectively surrounded the crystal with a black box except for the crystal faces at the end of the arms. Hence, light that entered one crystal face could exit only at a second crystal face. Figure 5 shows the shape of the crystal holder. As an added precaution, a blue filter was placed between the crystal and the camera to prevent visible radiations from the heater elements from reaching the film.

An overlap in scattering data between the high temperature and low temperature experiments provided a check on the reliability of the apparatus for the elimination of parasitic light.

The general technique used was to allow the temperature of the crystal to reach the desired value and to remain at that value for a few minutes until equilibrium had been reached and then to measure the intensity of the light scattered by the alkali halide for scattering angle $2\theta = 90°$. To make certain that equilibrium had been reached and to insure that we were not measuring a transitory effect, the crystal was held at the desired temperature for several hours. At different intervals of time, the scattering power was measured and recorded. This was done over the entire range of temperatures investigated and for all the samples used.

The samples of alkali halides (KCl, NaCl, and KBr) were obtained from the Harshaw Chemical Company. Two of the samples (NaCl and KCl) had been investigated by Plint, Theimer, and Sibley (11) over a limited temperature range in 1958. No experimental work had been performed on the KBr sample.

Since the photographic method of detection was used for measuring the scattering intensity, the film must be calibrated against the light source for the proper exposure time. To do this, the direct beam suitably attenuated passed through a seven step density filter, which was placed between source and film. A microphotometer was used to compare the densities of the seven steps, and from this data an H-d curve of photographic density versus log intensity was calculated. To avoid conflict with the reciprocity law, the calibration exposure time was the same as the exposure times used in the experiment.

Kodak Royal Pan film was used, since it is very sensitive in the spectral range under consideration. The data were evaluated with a Leeds and Northrup recording microphotometer.

A precaution that helped cut down experimental error and false interpretation of data was the simultaneous development and processing of all data corresponding to a particular experimental run. Hence effects due to poor microphotometer adjustment or developing procedure would be the same for all parts of a given experiment.

Time Changes

In this phase of the experiment, the crystal was brought to the desired temperature and the scattering intensity at $2\theta = 90°$ was measured. The crystal was then held at this constant temperature for a period of one hour and the scattering intensity again measured. This process was repeated each hour for four hours. A graph of intensity versus time would then show the effect of time changes upon the scattering power. The object of our time change experiments was to determine whether the "fast structure" and "slow structure" observed by Taurel and Humphreys-Owen (13) for imperfections in quartz is in fact also present in crystals of the alkali halides.

Heat Treatments

For this phase of investigation, which covered a temperature range from room temperature to within about 50 degrees of the melting point of the crystal, i.e. approximately 760° C., the technique used was to slowly heat the crystal up to the desired temperature; then hold at this temperature until equilibrium had been attained; and then to measure the intensity

of the scattered light flux. After the scattering intensity had been measured, the crystal was allowed to cool slowly to room temperature while still in the scattering box. This slow cooling supposedly does not introduce dislocations into the crystal.

The crystals were also subjected to a fast quench from high temperatures; and, after being cooled to room temperature, the scattering power was measured. This was done in an attempt to duplicate scattering data collected by previous experimenters (24) on similar crystals.

In the fast quench treatment, the same crystal was successively heated and quenched from temperatures near room temperature to values very near the melting point of the crystal. The crystal was held at the appropriate temperature for two hours and then air quenched to room temperature.

Etch Pit Analysis

The crystals were also chemically etched and a dislocation etch-pit count made. For this purpose the samples were divided into three classes:

1. "as grown" crystals
2. crystals after the high temperature equilibrium treatment, i.e. annealed crystals
3. crystals after the high temperature quench treatment.

In the above three classes it should be noted that all three came from the same crystal. Before any experiments were made, a small piece was cleaved from the end of one of the arms of the crystal. After the crystals had been annealed from 650° C., a second piece was cleaved from the same arm. Then the crystals were subjected to fast quench treatment

and a third piece was cleaved as before.

The technique used in this experiment was in principle the same as that of Sakamoto and Kabayashi (25), although different etchants and rinses were required for the three crystal materials. The crystal was etched for a few seconds and then rinsed. The wet crystals were then dried on blotting paper and the etch pits photographed through a microscope. From the photographs, a dislocation density was determined.

For KCl, the etchant used was a mixture of methanol and acetic acid that had been saturated with zinc ions. The crystal was etched for 30 seconds and then rinsed in 0.5% solutions of mercuric chloride in acetone. The pits were very sharp and clear and could be photographed with no difficulty. Several spots were picked at random on the etched surface, photographed, and an etch pit count made. Etch pit counts were made on all three samples of KCl, i.e. "as grown" crystals, annealed crystals, and crystals subjected to fast quench.

For NaCl a desirable etchant was found in absolute ethyl alcohol containing 3 gms./liter of $HgCl_2$ as inhibitor. The rinse was the same as used for KCl. The etch pits were not as clear and sharp as for KCl.

Since KBr dissolves quite readily in water, one must be quite selective in picking a rinse. In addition, most etchants have a peculiar effect in that some dislocations are etched preferentially yielding deep etch pits whereas others form only shallow pits that can be seen only with great difficulty and then oblique lighting must be used. Glacial acetic acid was used as etchant. The crystal was etched for three seconds, then rinsed in CCl_4 and shaken dry. The pits were very shallow and were not suitable for photography.

Impurity Analysis

Semi-quantitative flame photometric analysis of the specimens was performed through the courtest of Dr. W. A. Sibley of the Oak Ridge National Laboratory, and is considered to be accurate to 30%. The list on Table II shows not only the impurities found in the samples under investigation, but also the impurities sought for and not found. The total divalent ion impurities present in the specimens are:

$$NaCl < 2 \cdot 10^{-6}$$

$$KCl < 4 \cdot 10^{-6}$$

$$KBr < 3 \cdot 10^{-6}$$

It should be noted that Al enters the lattice as Al^{++} (26).

Neutron activation analysis could also have been used. However the nuclear reactor available for this experiment has a very low neutron flux, and with the low concentration of impurity in the samples investigated, this method would not have been much of an improvement over the flame photometric method.

TABLE II

ELEMENT	LIMIT OF DETECTION	KCl	KBr	LIMIT OF DETECTION	NaCl
Ag	0.0002 %	–	–	0.00027 %	–
Al	0.00083	< F	–	0.0007	–
As	0.42	–	–	0.37	–
Au	0.00097	–	–	0.0059	–
B	0.008	–	–	0.012	–
Ba	0.018	–	–	0.024	–
Be	0.00007	–	–	0.00011	–
Bi	0.002	–	–	0.0011	–
Ca		< F	< F		< F
Cd	0.056	–	–	0.049	–
Co	0.0002	–	–	0.0017	–
Cr	0.00024	–	–	0.0003	–
Cu	0.00013	–	–	0.00016	–
Fe	0.0025	–	–		F*
Ga	0.0016	–	–	0.0012	–
Ge	0.0056	–	–	0.0048	–
Hg	1.2	–	–	2.8	–
K		A	A	0.92	–
Li	0.014	–	–	0.0044	–
Mg	0.00077	< F	< F	0.00009	< F
Mn	0.00077	< F	< F	0.0009	–
Mo	0.0011	–	–	0.0017	–
Na	0.07	–	–		A
Ni	0.0012	–	–	0.0008	–
P	0.32	–	–	0.38	–
Pb	0.012	–	–	0.0077	–
Pd	0.00083	–	–	0.0016	–
Pt	0.00093	–	–	0.0018	–
Ru	0.0037	–	–	0.012	–
Sb	0.033	–	–	0.04	–

TABLE II CONTINUED

ELEMENT	LIMIT OF DETECTION	KCl	KBr	LIMIT OF DETECTION	NaCl
Si	0.005 %	–	–	0.005 %	–
Sn	0.0032	–	–	0.0032	–
Sr	0.038	–	–	0.047	–
Ta	0.09	–	–	0.033	–
Te	0.4	–	–	0.26	–
Ti	0.0024	–	–	0.0019	–
Tl	0.021	–	–	0.016	–
V	0.0011	–	–	0.0012	–
W	0.068	–	–	0.029	–
Zn	0.40	–	–	0.32	–
Zr	0.0033	–	–	0.0012	–

SYMBOLS:

A 10–100%
F 0.0001–0.001%
– Sought, but not found

*A check on the iron concentration in Sodium Chloride by ESR techniques revealed no trace of iron. Accordingly, we assume that this flame photometric analysis is in error at this point.

CHAPTER V

EXPERIMENTAL RESULTS

Low Temperature Results

The low temperature results cover the temperature range from -100° C. to 200° C. In this range the equilibrium scattering power versus temperature was measured for alkali halide crystals of type KCl, KBr, and NaCl. Results of these measurements are shown in Figures 6, 7, and 8. In each case a prominent peak appears in the scattering power. For NaCl the peak appears at about 273° K. For KCl and KBr the peaks were at 213° K and 223° K respectively. The increase in the scattering power on the low temperature side of the peak appears to be an exponential increase as can be seen when the natural logarithm of the scattering power is plotted against 1000/T. However this experimental range is so short that it is quite difficult to tell whether the curve should be exponential or a similar type. The drop off on the high temperature side of the peak is also an exponential. Figures 9, 10, and 11 show the results of the low temperature equilibrium scattering.

The slope of the logarithmic graph on the low temperature side of the peak is approximately the same for the three samples, viz: -0.50 for KCl, -0.56 for KBr, and -0.55 for NaCl.

On the high temperature side of the peak, the plot of $\ln P$ versus 1000/T again is a straight line for each of the samples investigated,

the slopes being 0.33, 0.31, and 0.64 for KCl, KBr, and NaCl respectively. The low temperature region covered the range up to a temperature of 200° C, but in each case the high temperature data fits smoothly to the low temperature data in the range where the temperatures overlap. This overlap in data occurs for measurements in the temperature range from room temperature to 200° C.

The low temperature peaks in the scattering power are caused by processes that appear to be reversible. When the temperature was repeatedly cycled between -100° C and 200° C, the peaks still appeared in the same place and all details of the graphs could be reproduced.

In the low temperature range where scattering peaks are prominent, a measurement of possible time changes in the scattering power gave negative results over a period of five hours.

Figures 18, 19, and 20 show the results for KCl, KBr, and NaCl for temperatures from -100° C up to about 200° C. In this low temperature range there does not appear to be a time change in scattering power, however, these experiments covered a range of only about five hours rather than the eighty hours used by taurel (13). It must be pointed out that Taurel's experiments showed that about 70% of the total change occurred during the first 8 to 10 hours. If a similar change occurred for the alkali halides investigated here, it should have been noticable over our experimental range.

High Temperature Results

In the high temperature range from room temperature to within 50 degrees of melting, the scattering power versus temperature data fall into two distinct ranges. In the first range the curve of lnP versus

1000/T fits smoothly onto the low temperature data in the overlap range from room temperature to 200° C. This line continues with the same slope until about 500-600° C, although the exact break-point varies from material to material. Above the break the curve drops off sharply to an extremely low value within a 50 degree temperature range for all three samples. The drop is so rapid that an accurate determination of the slope is not possible.

The ratio of peak height to height at 600° C was 5.6, 13.0, and 6.4 for KCl, KBr, and NaCl respectively. The value for KBr is almost two times that of KCl or NaCl. It may be noted that KBr also behaves differently from KCl and NaCl in the range between the scattering peak and 600° C. Whereas the data for both KCl and NaCl lie on a straight line when lnP was plotted against 1000/T, the KBr data lay on two straight lines of slightly different slope. This may be seen by comparison of Figure 10 with Figures 9 and 11. The data for KCl and NaCl do show a slight tendency to lie on two straight lines, but it is much less pronounced than for KBr.

The processes causing the change in high temperature equilibrium scattering power were also reversible. When the temperature was cycled between room temperature and 650° C, the above data was reproduced. In fact, the entire process from -100° C to 650° C appears to be reversible. This was shown by observing the low temperature peaks after the high temperature experiments were completed. The low temperature peaks reappeared in their proper positions for all three samples.

Fast Quench

After the equilibrium scattering power dependence upon temperature was investigated in the range -100° C to 650° C, the crystals were

subjected to a fast quench treatment.

The high temperature quench results may be classified into two obvious regions and a third possible region that is not quite so obvious. The first region terminates at about 490° C, 450° C, and 561° C for KCl, KBr, and NaCl respectively. These breaks become obvious when one plots lnP versus 1000/T for the three samples. On the low temperature side of the break, the fast quench curves have slopes 0.20, 0.60, and 0.40 for Kcl, KBr, and NaCl respectively. These values are to be compared with the values 0.33, 0.31, and 0.64 obtained for these same crystals at equilibrium scattering temperatures.

On the high temperature side of the break, the scattering power increases very quickly in contrast to the slow, steady decrease when equilibrium conditions are met. For KCl, KBr and NaCl, the slopes turn out to be -4.4, -3.0, -3.33. The point where the fast quench curve rises sharply upward is roughly the same as the point where the equilibrium curve drops sharply. For fast quench, the point is at 492° C, 452° C, and 561° C for KCl, KBr, and NaCl. These values are to be compared to 490° C, 492° C, and 560° C for equilibrium treatments. These values for equilibrium measurements of break point are not as accurate as these for the fast quench because of the small number of data points available. At points dangerously near the melting point of the crystals, the quench treatment showed a rapid decrease in scattering power. Not enough data points were available to measure the slope or to determine with any accuracy the temperature at which the drop started. Figure 21 illustrates the quench treatment data.

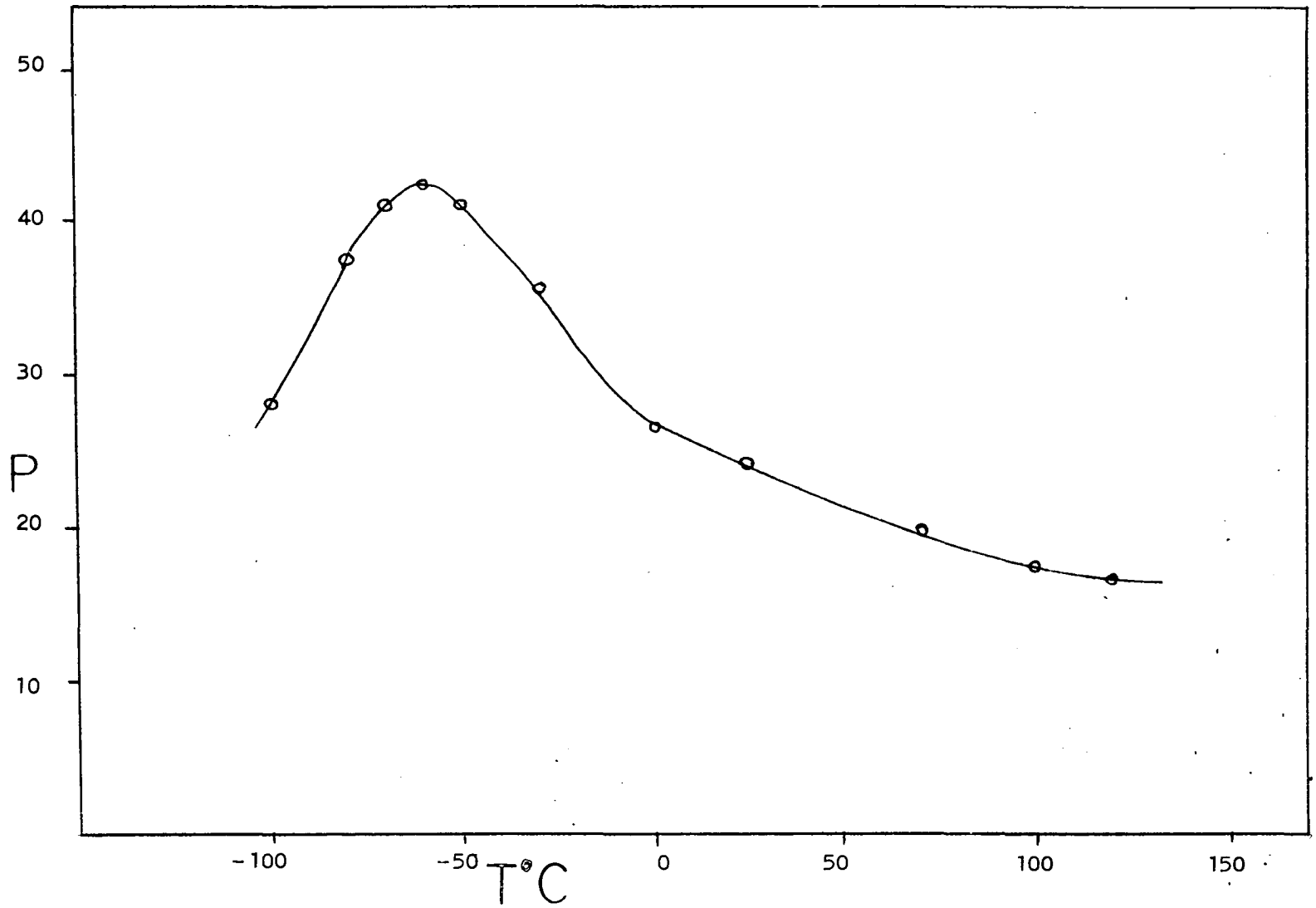

Fig. 6.--Low Temperature Scattering Power For KCl

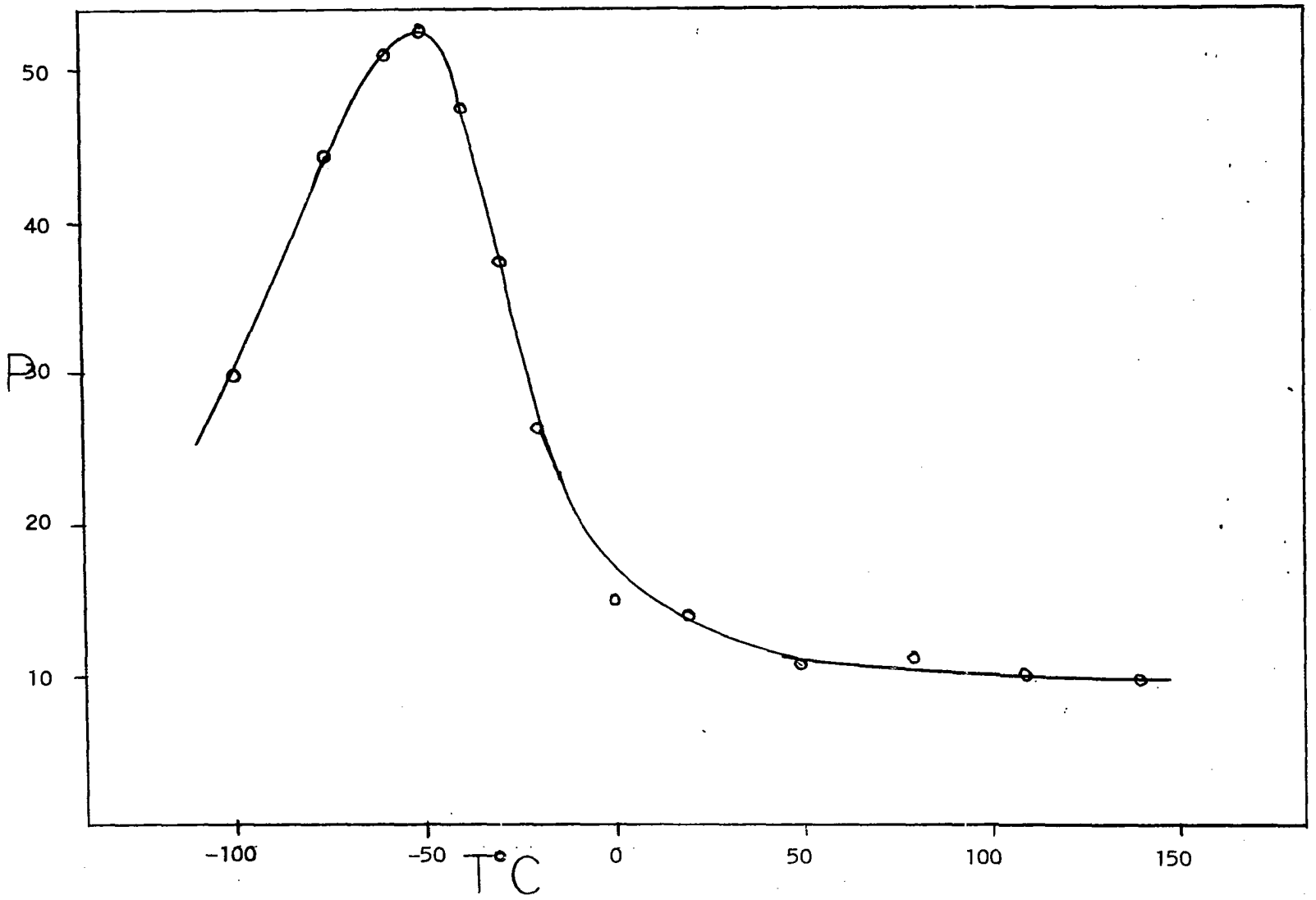

Fig. 7.--Low Temperature Scattering Power For KBr

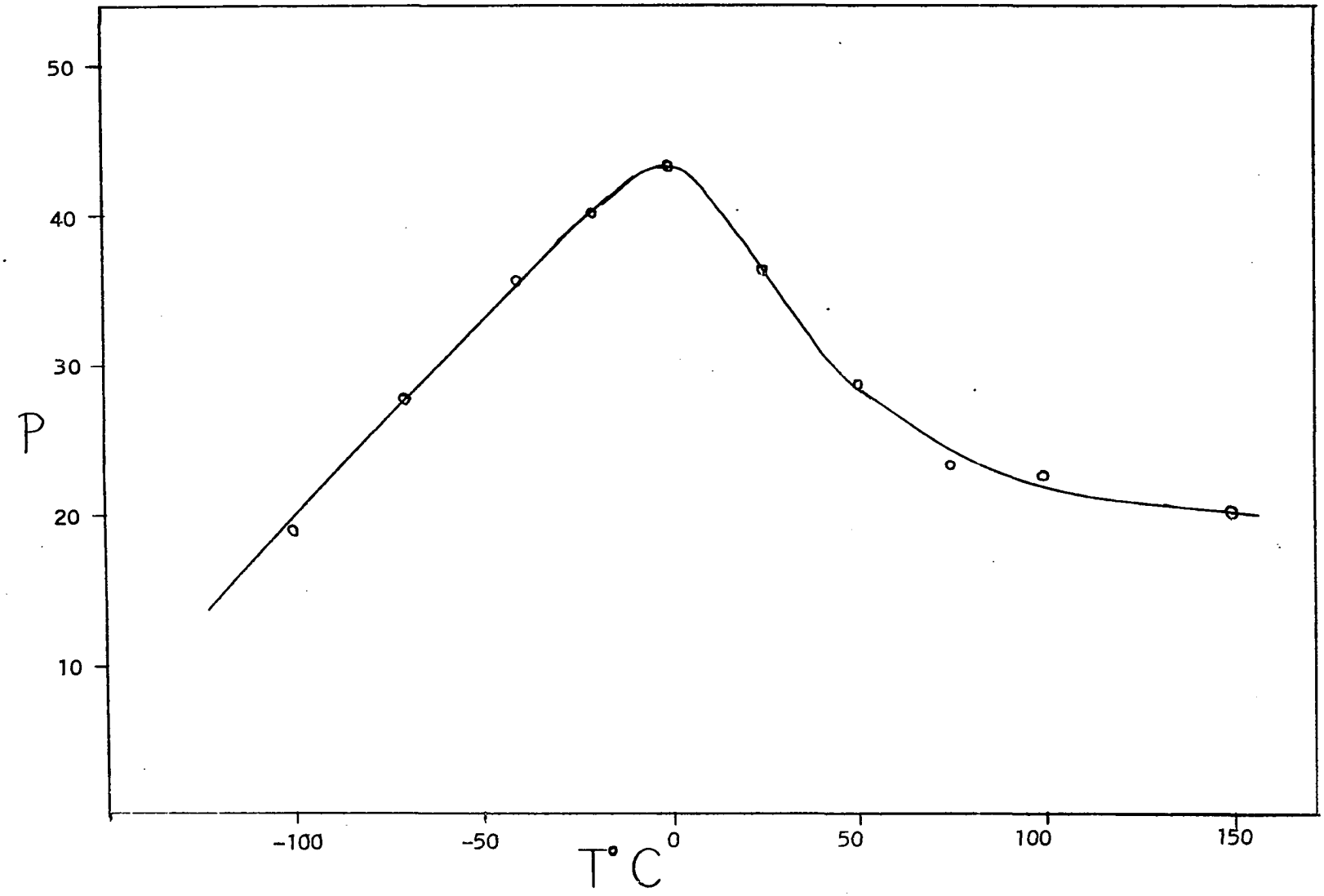

Fig. 8.—Low Temperature Scattering Power For NaCl

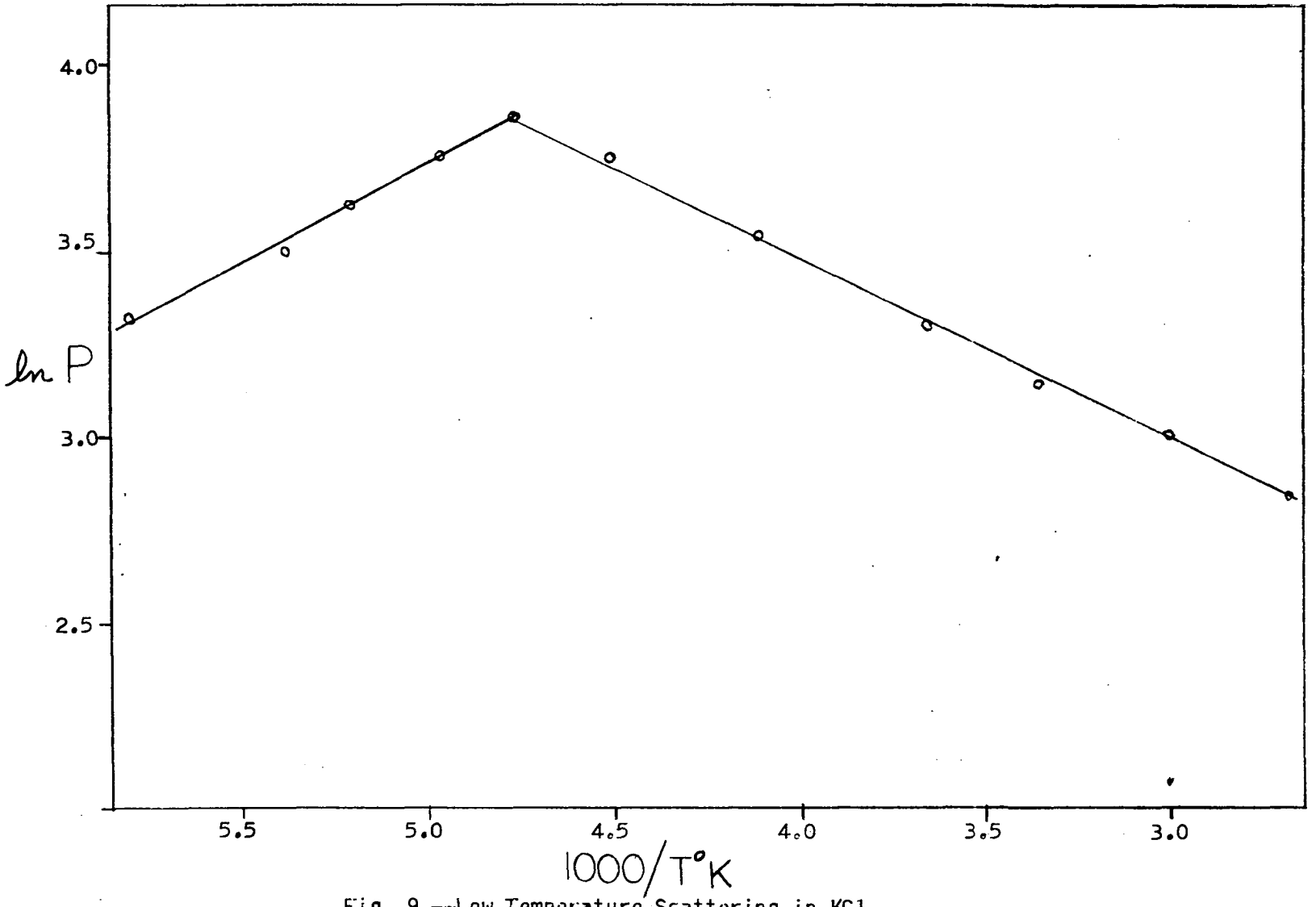

Fig. 9.--Low Temperature Scattering in KCl

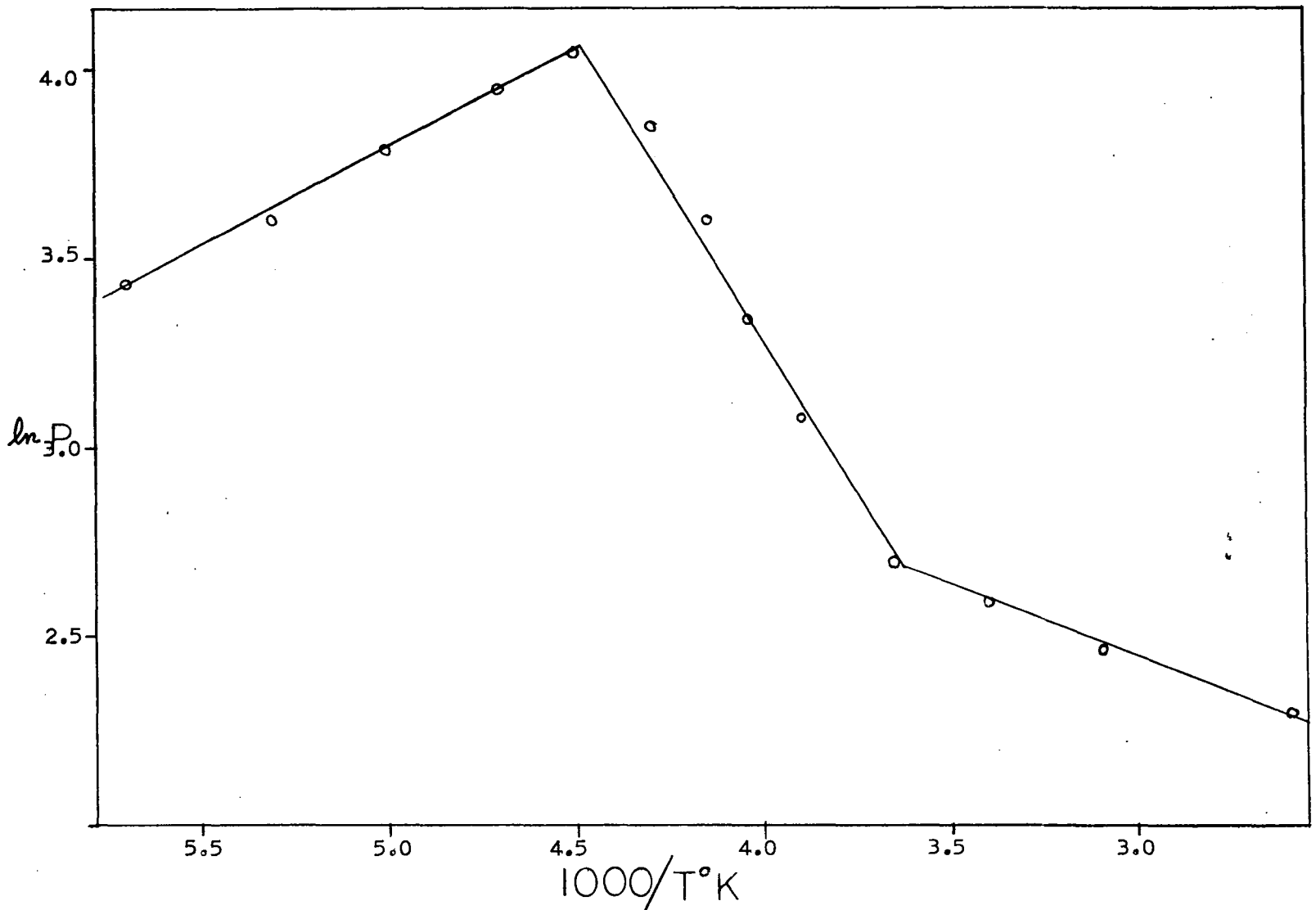

Fig. 10.--Low Temperature Scattering in KBr

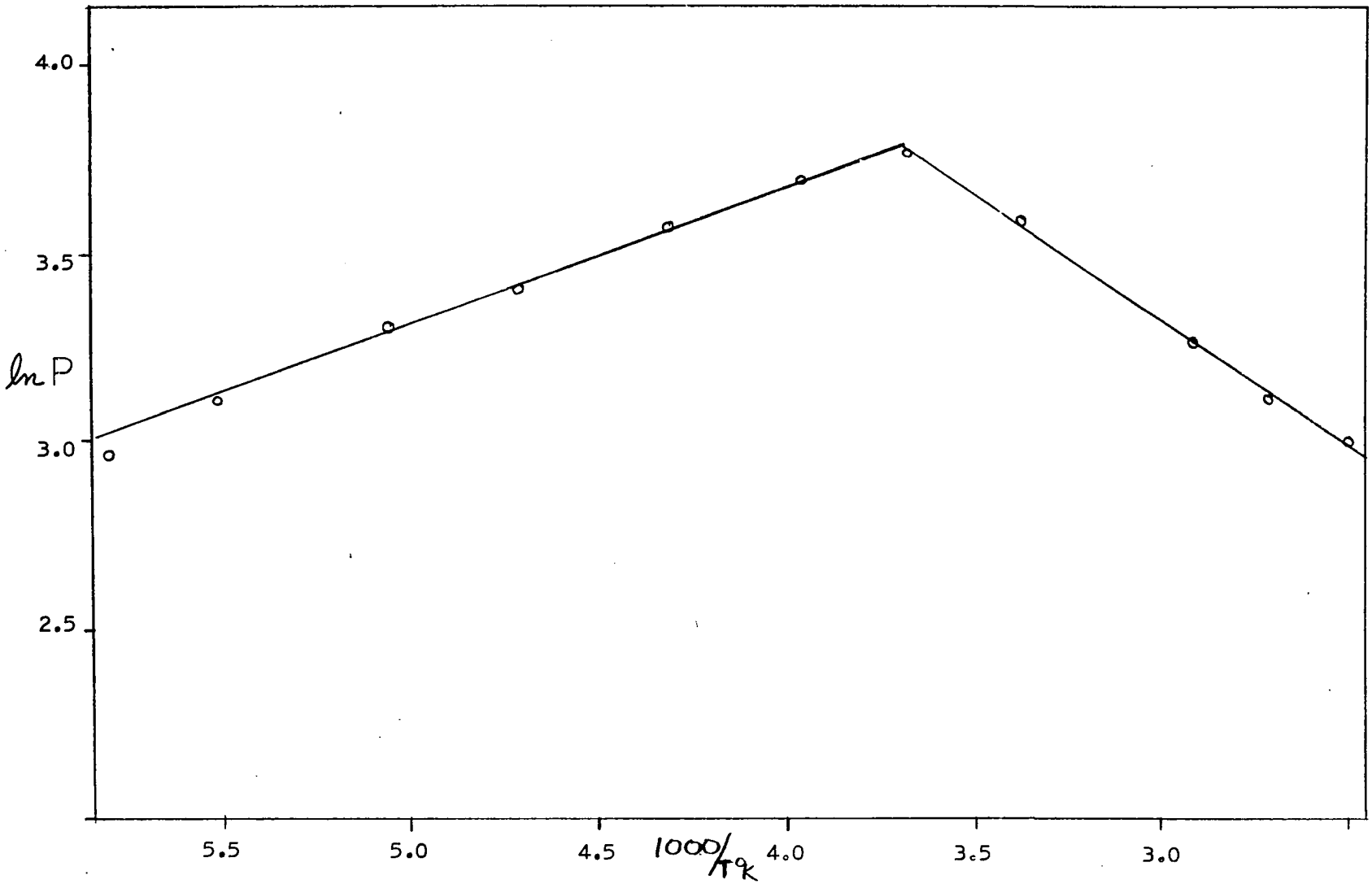

Fig. 11.--Low Temperature Scattering in NaCl

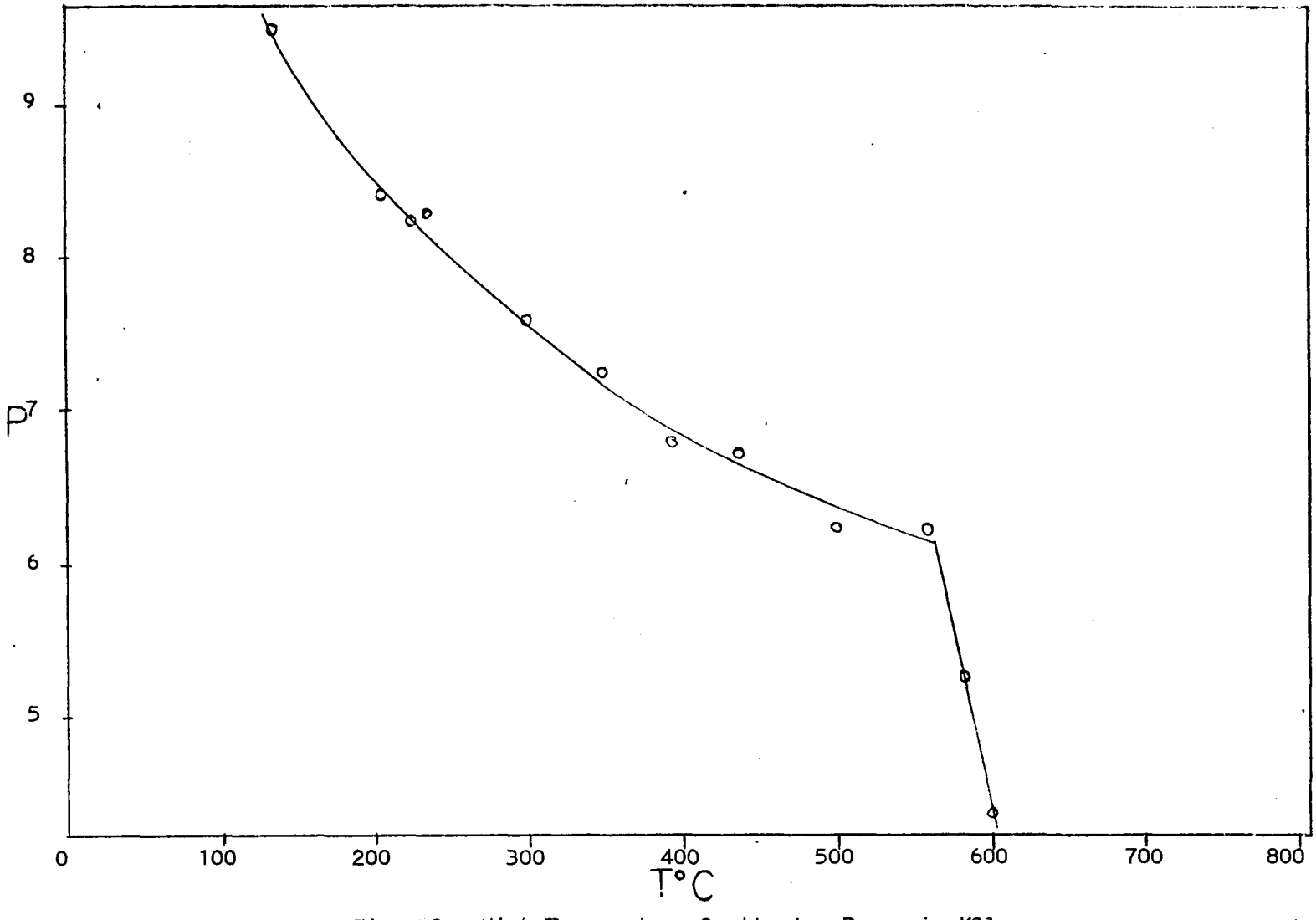

Fig. 12.—High Temperature Scattering Power in KCl

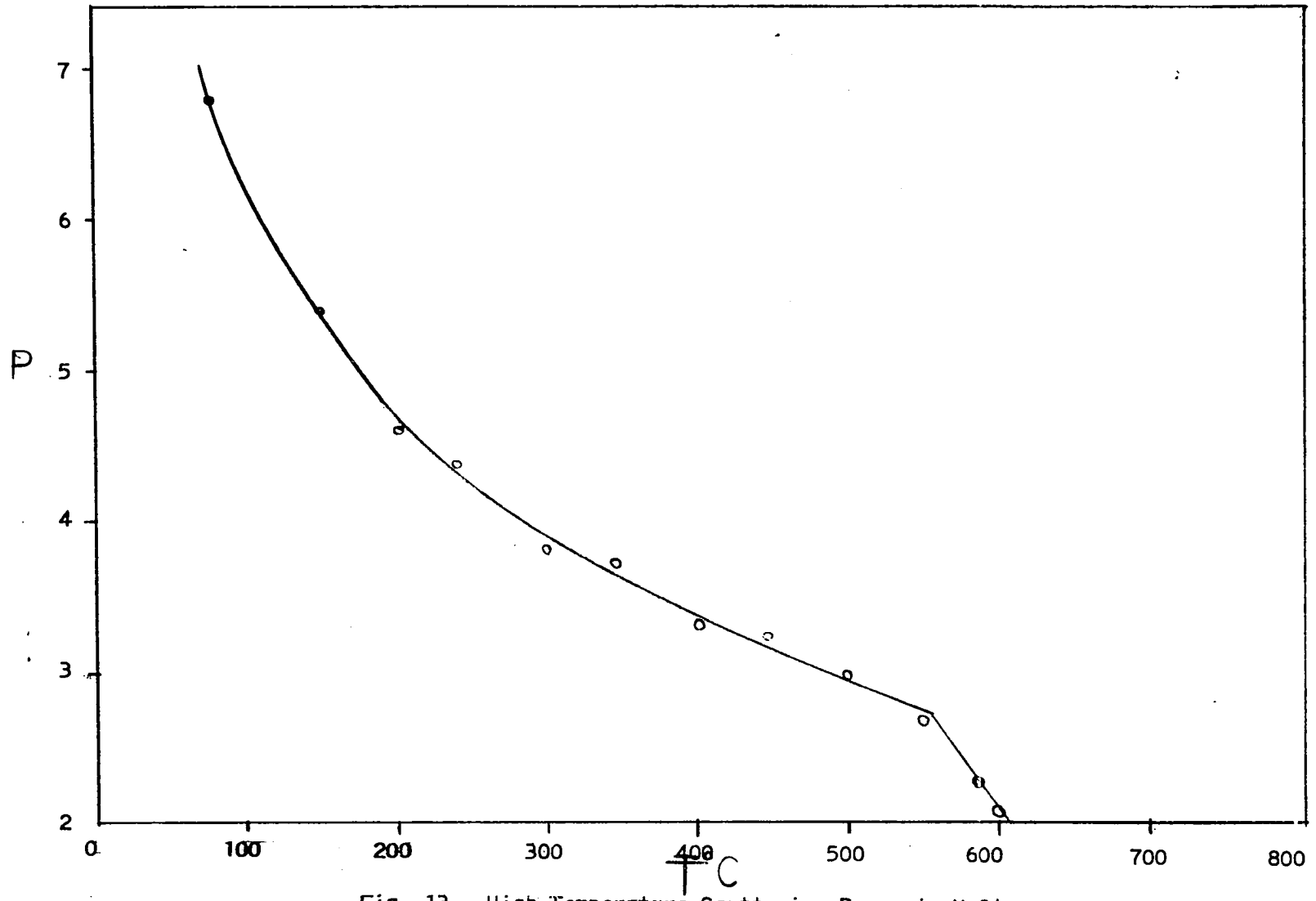

Fig. 13.---High Temperature Scattering Power in NaCl

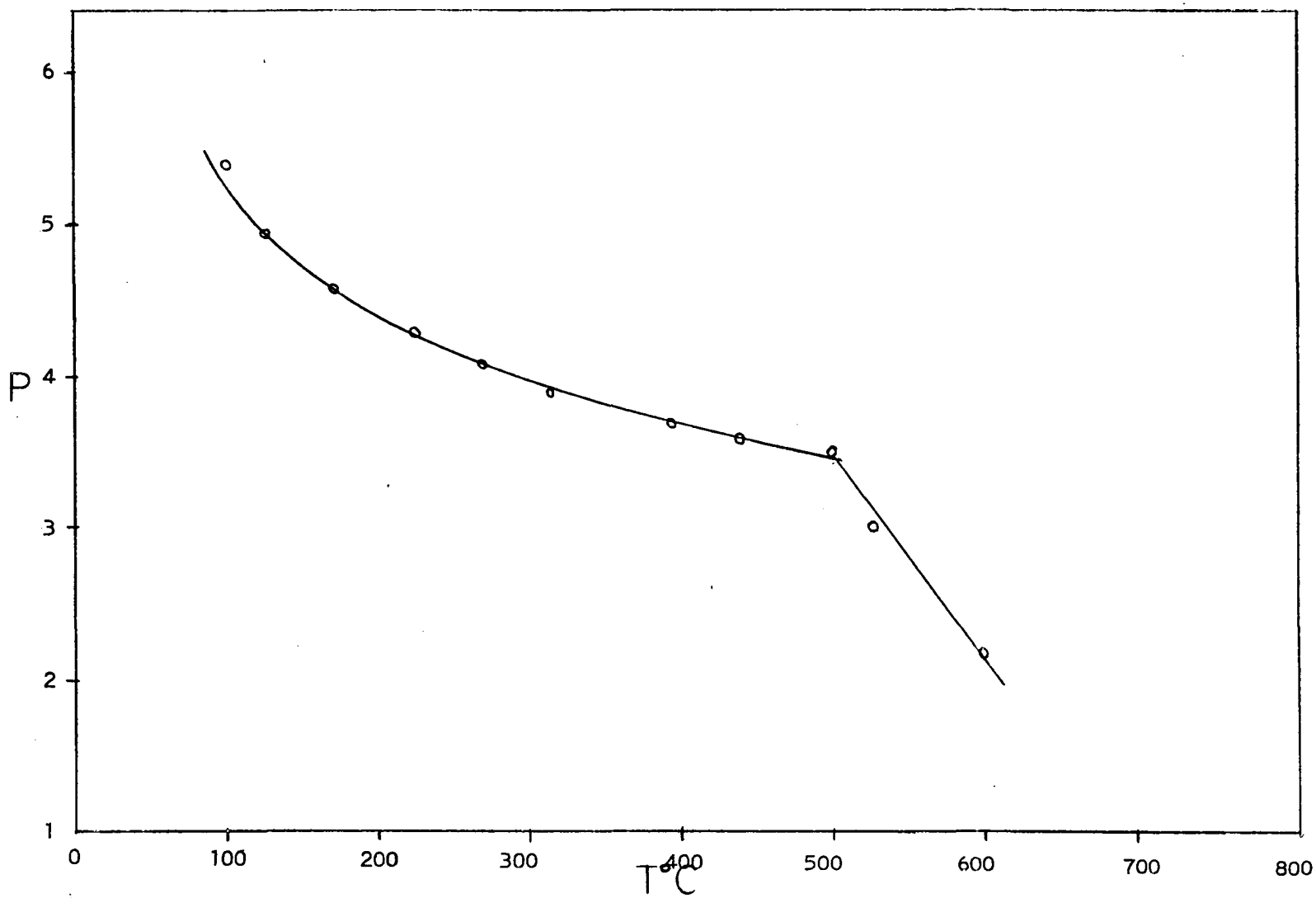

Fig. 14.—High Temperature Scattering Power KBr

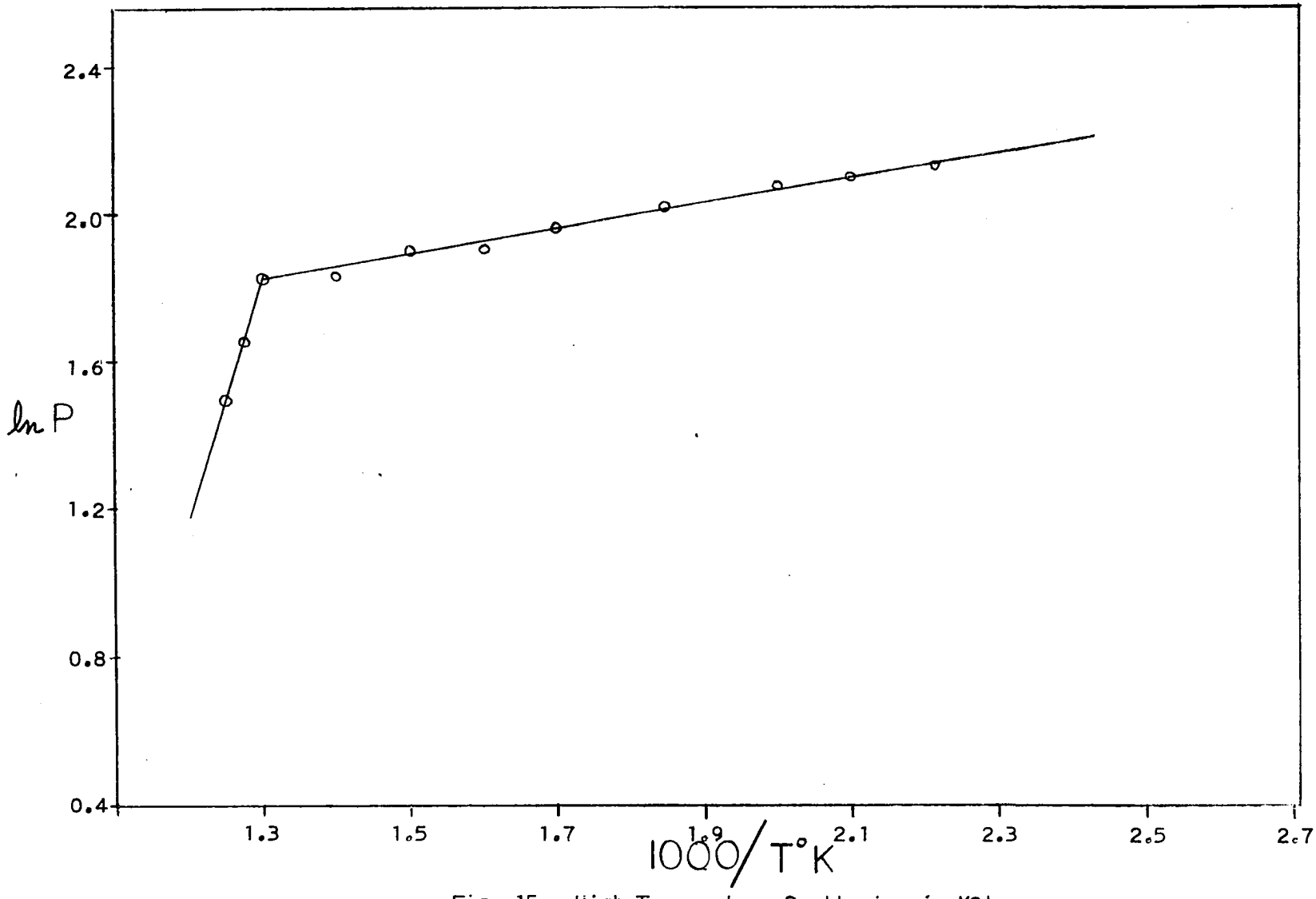

Fig. 15.—High Temperature Scattering in KCl

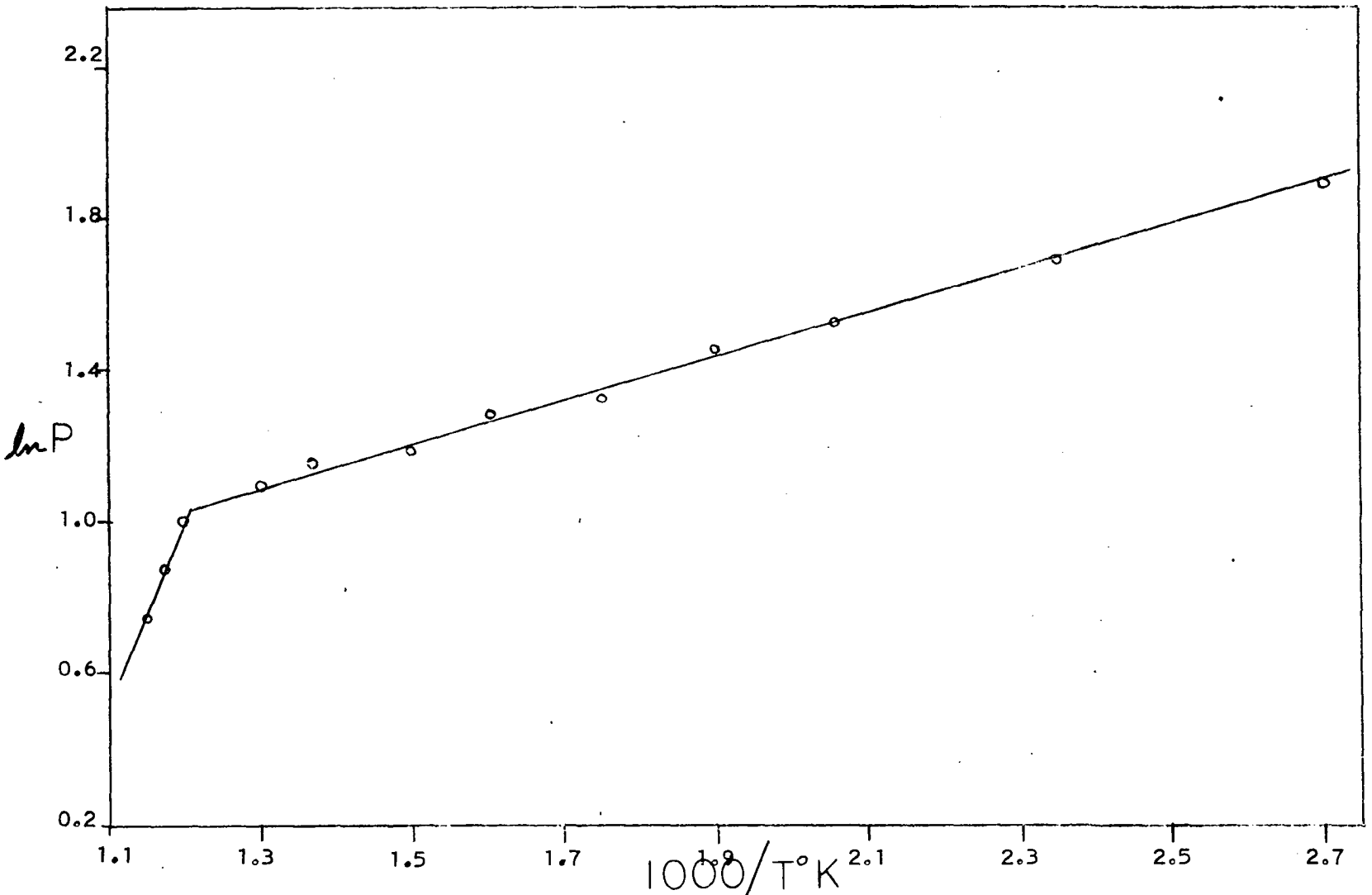

Fig. 16.--High Temperature Scattering in NaCl

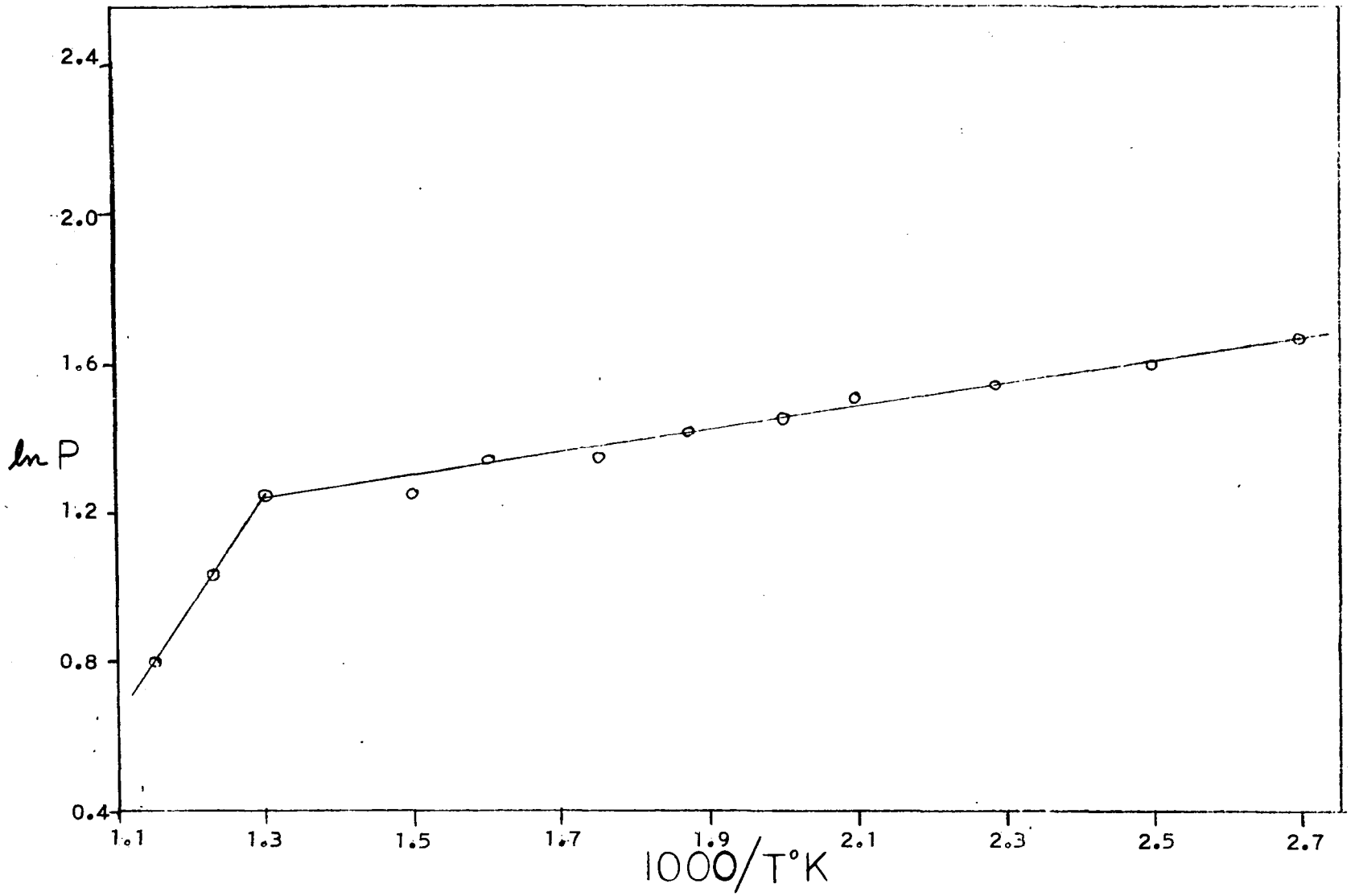

Fig. 17.--High Temperature Scattering in KBr

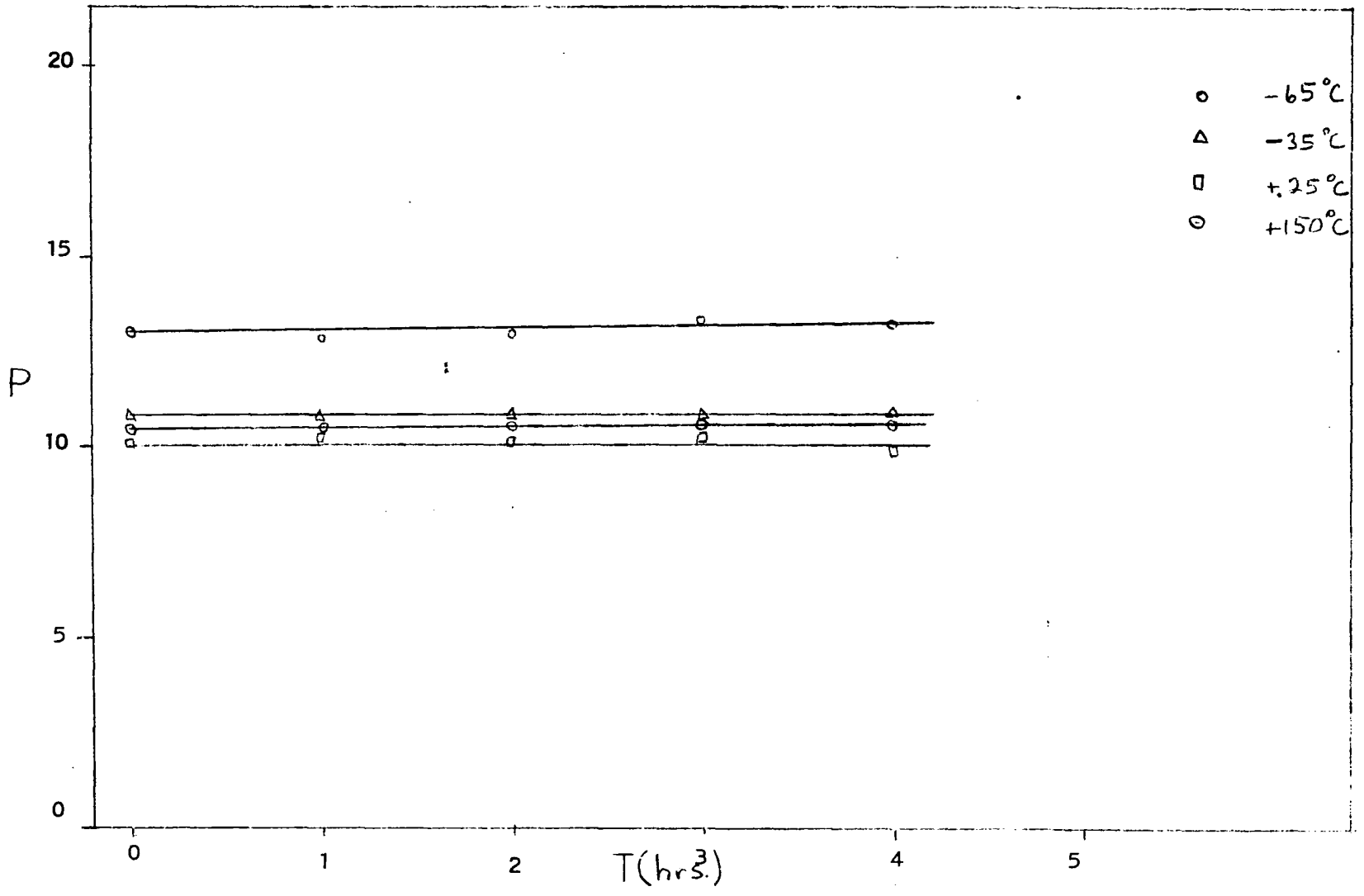

Fig. 18.—Time Changes in Scattering Power—KCl

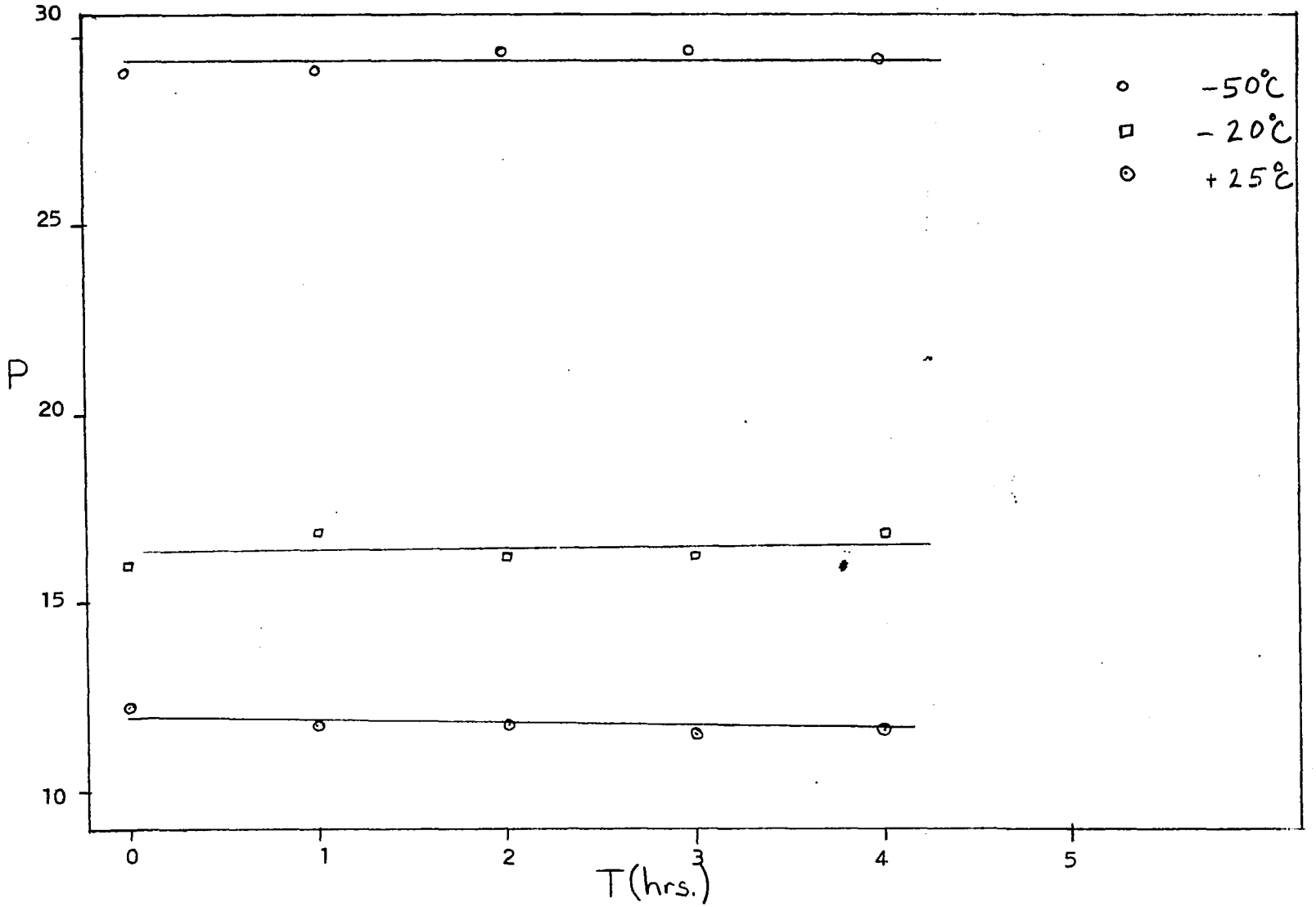

Fig. 19.—Time Changes in Scattering Power-KBr

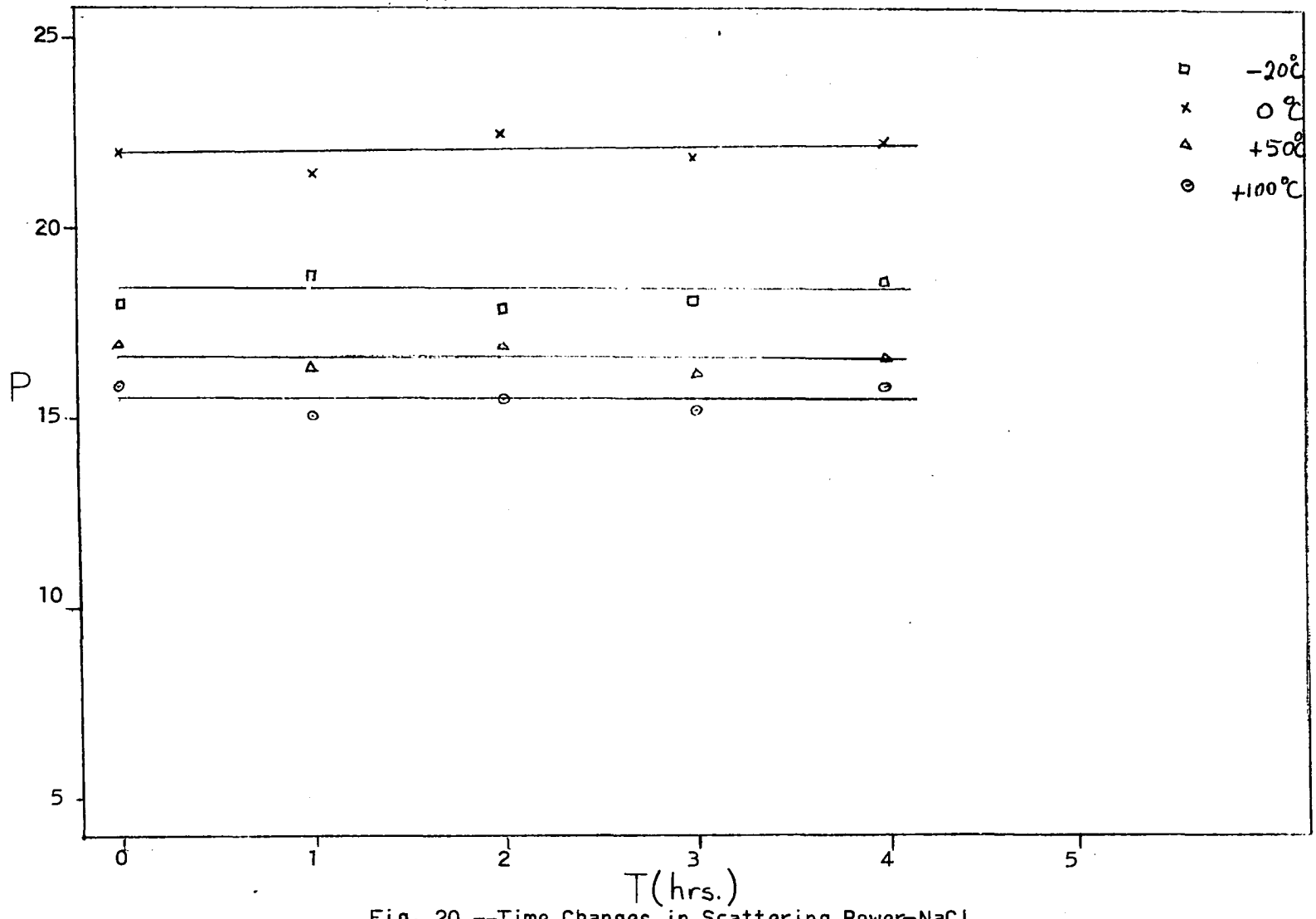

Fig. 20.--Time Changes in Scattering Power-NaCl

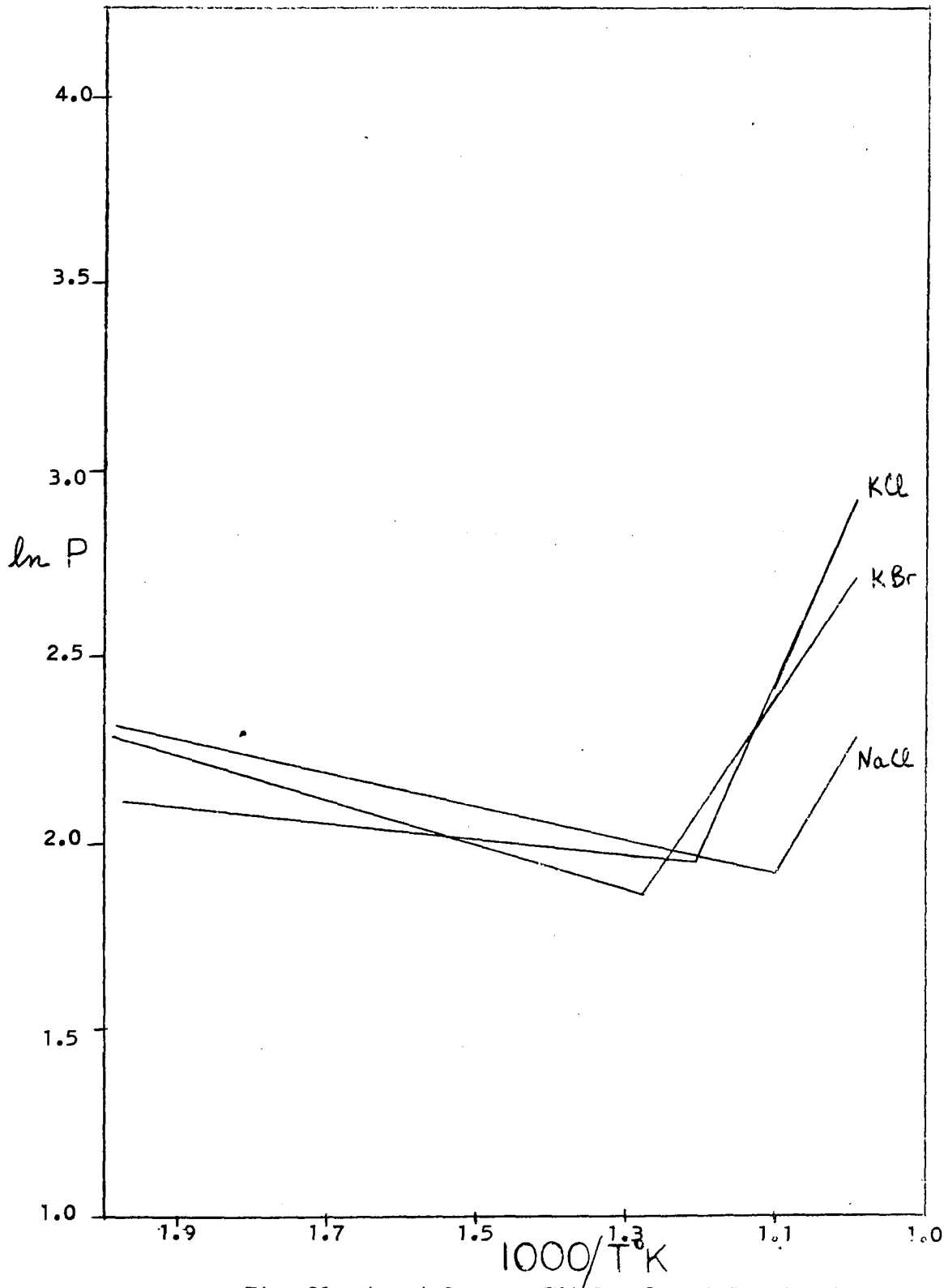

Fig. 21.--Least Squares Fit For Quench Treatment

Etch Pit Analysis

Results for KCl are shown in Figures 22 and 23, where etch pit pictures are shown, and Table III, which shows the density of dislocations through a (100) plane. The dislocation density for annealed KCl has increased by a factor of four over the "as grown" crystal. Likewise, the dislocation density for fast quenched crystal has increased by a factor of ten over the "as grown" crystal.

No significant change in the dislocation pattern between the "as grown" KCl and the crystals heated as high as 650° C and slowly cooled was observed. A slight piling up of dislocations near grain boundaries and a density increase appears to have occurred in the annealed crystals.

When one compares the annealed crystal with the fast quenched crystal, a drastic change is immediately apparent. Other than the larger concentration of dislocations that is present in the fast quenched crystal, a new phenomenon is now visible. This new phenomenon has the general appearance of a glide band except for its irregular directions. It appears to be a grain boundary with an enormous number of dislocations in close proximity. The dislocations are so closely packed in this general area that accurate counting is impossible. This may be seen quite clearly in Figure 23.

The dislocation density for annealed NaCl was larger than "as grown" NaCl by a factor two, while that for the fast quenched crystal had increased by a factor of five over the density in the "as grown" crystal. A list of the dislocation densities for NaCl appears in Table III.

Large groups of dislocations were observed for KBr, but they were too shallow to photograph adequately.

TABLE III

CRYSTAL	DISLOCATION DENSITY	HISTORY
KCl		
	(1) $0.14 \times 10^6/cm^2$	As grown
	$0.125 \times 10^6/cm^2$	" "
	(2) $0.4 \times 10^6/cm^2$	Slow anneal
	$0.5 \times 10^6/cm^2$	" "
	(3) $1.0 \times 10^6/cm^2$	Fast quench
	$1.2 \times 10^6/cm^2$	" "
NaCl		
	(1) $0.14 \times 10^6/cm^2$	As grown
	(2) $0.26 \times 10^6/cm^2$	Slow anneal
	(3) $0.6 \times 10^6/cm^2$	Fast quench

"As grown" x 250

"Annealed" x 250

Fig. 22.--Etch Pits in KCl

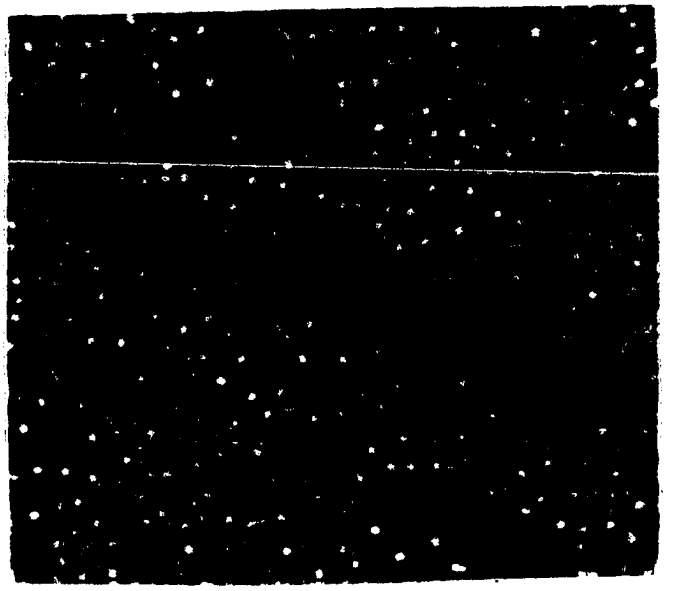

"Fast quench" x 250

Fig. 23.--Etch Pits In KCL

CHAPTER VI

CONCLUSIONS

The experiments and theoretical considerations of Theimer, Plint, and Sibley (9, 12) and recent results of Sibley (27) seem to indicate conclusively that the scattering centers in the alkali halide crystals produced by Harshaw are closely associated with dislocations. To be sure, one may expect formation of impurity precipitates at the nodes of a dislocation network, but it has been shown that the scattering from such centers displays an angular dependence that is markedly different from that of long cylindrical scatterers with definite crystallographic orientations. In view of these results we will assume, ab initio that our scattering centers are long cylindrical clouds of vacancies and impurities associated with dislocation networks.

The exact formula for the scattering power of such a center depends on the particular function chosen to represent the radial distribution of defects about the dislocation line. However, whatever function is chosen, a formula of the following type holds (11):

$$P(\theta\lambda) = 4\sigma(\theta\lambda)(n^*\alpha^* V^*)^2 \frac{\sin^2 \frac{\mu z}{2}}{\left(\frac{\mu z}{2}\right)^2} f(r^*) \qquad (48)$$

where $f(r^*)$ is a function of the effective radius r^*, n^* is the average concentration of point defects, and V^*n^* is the total effective number of point defects in a bad region, and the other terms are the same as

defined earlier.

In considering the temperature variation of the scattering from such a center, one notes that only the quantities n*, V* and r* are likely to change and that these quantities are interrelated (Koehler). It is possible that $n^*\alpha^*$ could change because of dissociation of vacancy-impurity pairs as the temperature is raised. A vacancy-impurity pair would have an effective polarizability less than that of a dissociated pair. If this mechanism operates to any appreciable extent the scattering should increase with temperature increase. The contrary effect is observed in that range of temperature for which dissociation could occur. It must not be supposed that dissociation does not happen but that the concentration of point imperfections in the cloud is determined by the mechanism discussed earlier for charged dislocations rather than a simple Boltzmann thermal equilibrium.

The total number of dislocations may vary with temperature but such an effect would not permit the reversibility of the equilibrium experiments that was observed. Furthermore, the small increase in etch pit count observed after cycling the temperature of a crystal could well be accounted for by the formation of small dislocation loops near the crystal surface. Such an effect has been observed for LiF by Gilman and Johnston (8).

Variations in V* and r* are distinctly possible if we accept the theory of charged dislocations outlined earlier. Accordingly, we shall attempt to examine the results in the light of the theory of charged dislocations.

Equilibrium Results

Each of the three samples used shows a prominent peak in the

scattering power versus temperature curve. We have noted earlier that for NaCl with divalent impurity concentration 10^{-6} this peak appears at approximately 273° K. Koehler has shown that for NaCl at moderately low average impurity concentration (i.e. about $3 \cdot 10^{-6}$) the impurity concentration at the core saturates at room temperature. By using the theoretical value $E_F = 0.66$ ev for energy of formation of positive ion vacancies in NaCl given by Koehler and also equation 18 of chapter 3, one obtains the result that at about 273° K with impurity concentration 10^{-6} the divalent ion concentration at the dislocation core should just drop below saturation. It thus seems plausible that the observed peak in scattering power is associated with the onset of saturation of impurities at the dislocation core. Obviously, we can apply the same reasoning to predict the energy of formation of positive ion vacancies in KCl and KBr since these crystals also show pronounced peaks in scattering power versus temperature. For KCl and KBr the peaks appeared at 213° K and 223° K respectively, and the energies of formation of positive ion vacancies for these halides are then calculated to be 0.42 ev and 0.46 ev respectively. The correct values for these alkali halides is not known with any degree of accuracy, experimentally or theoretically, but are believed to be in this neighborhood.

Mott and Littleton (23), for example, have calculated the energy of vacancy formation for KCl and KBr, and obtained values close to 0.85 ev, whereas the values obtained here are approximately one half of these values. The answer to this discrepency is undoubtedly connected with the uncertainty in the values of the impurity concentration. If the impurity concentration were larger than the estimated value, for example 10^{-5}, the appearance of a peak at 213° K for KCl would imply that the

activation energy is 0.4 ev., while an impurity concentration of 10^{-7} under the same conditions would imply an activation energy of 0.8 ev. This range of values for the formation energy is more than enough to explain the differences. Therefore, the impurity concentration must be known very accurately if results for the energies are to have any exact quantitative significance. It seems worthwhile to attempt to obtain more accurate knowledge of the concentrations in order to exploit this method for obtaining E_F^+.

In the following discussion it will be assumed that the peaks in scattering power are in fact associated with the onset of saturation of divalent impurities at the dislocation core.

In the region above the saturation peak a scattering power of the form

$$P = \frac{A}{T-T_0} \tag{49}$$

fits the experimental data quite well. Evaluating the constants in equation 49 for the three materials investigated, one obtains the following equations:

I. For NaCl $$P = \frac{5.17 \times 10^3}{T - 164} \tag{50}$$

II. For KCl $$P = \frac{4.85 \times 10^3}{T - 104} \tag{51}$$

III. For KBr $$P = \frac{1.38 \times 10^3}{T - 220} \tag{52}$$

The scattering power versus temperature has the same general shape above and below the saturation peak and hence a curve of the same type should fit both sides. For the region below the saturation peak the equations are:

IV. For NaCl $$P = \frac{-4.86 \times 10^3}{T - 377} \tag{53}$$

V. For KCl $$P = \frac{-2.85 \times 10^3}{T - 269} \quad (54)$$

VI. For KBr $$P = \frac{-3.95 \times 10^3}{T - 280} \quad (55)$$

The scattering power is, of course, always positive. Figures 24, 25, and 26 show the experimental values of P versus T, and also the values calculated using equations 50, 51, and 52 above. The results are in quite good agreement. Similar good agreement is found for temperatures below the peak.

If one attempts to use basic arguments and obtain a scattering power formula that closely resembles the experimental data, one must take into account simultaneously all the possible processes that could occur. Such a study is almost impossible, but by limiting oneself to one or two of the possible processes, perhaps one can get at least a qualitative idea of the relative importance of each process in the production of changes in the scattering light flux.

The most important single item appears to be the concentration of divalent impurities. We shall focus our attention for the present upon the effects due to these impurities.

Let us suppose that in the region below the saturation peak the divalent impurity concentration is not a constant but varies with temperature. For example, the divalent impurity could be precipitated into a new phase at the low temperatures. We shall assume with Eshelby et. al., that below the saturation peak the divalent impurity concentration in solid solution in the crystal varies somewhat as

$$C = A\, e^{-B/kT} \quad (56)$$

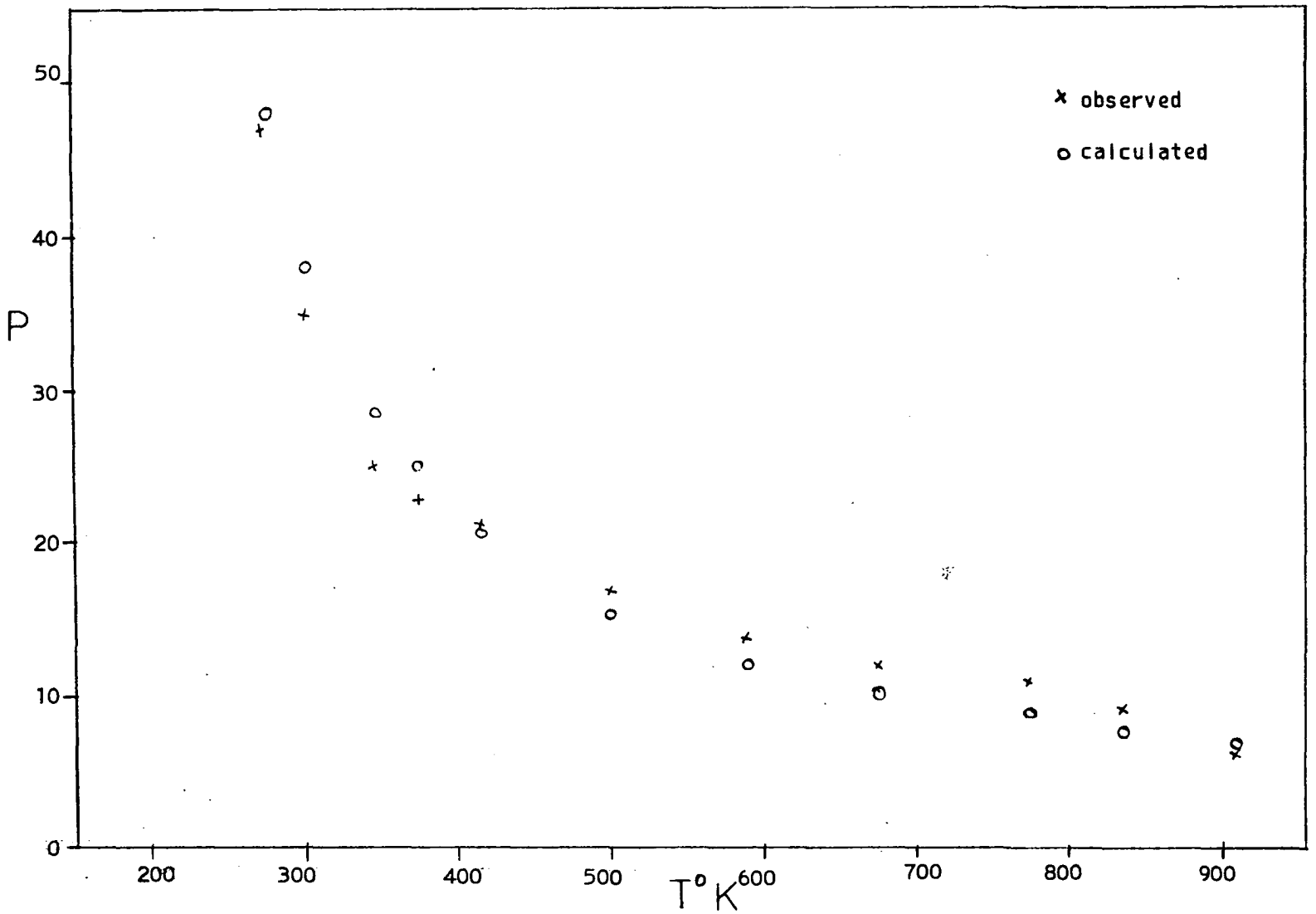

Fig. 24.--Comparison of Empirical Values With Experimental Values = NaCl

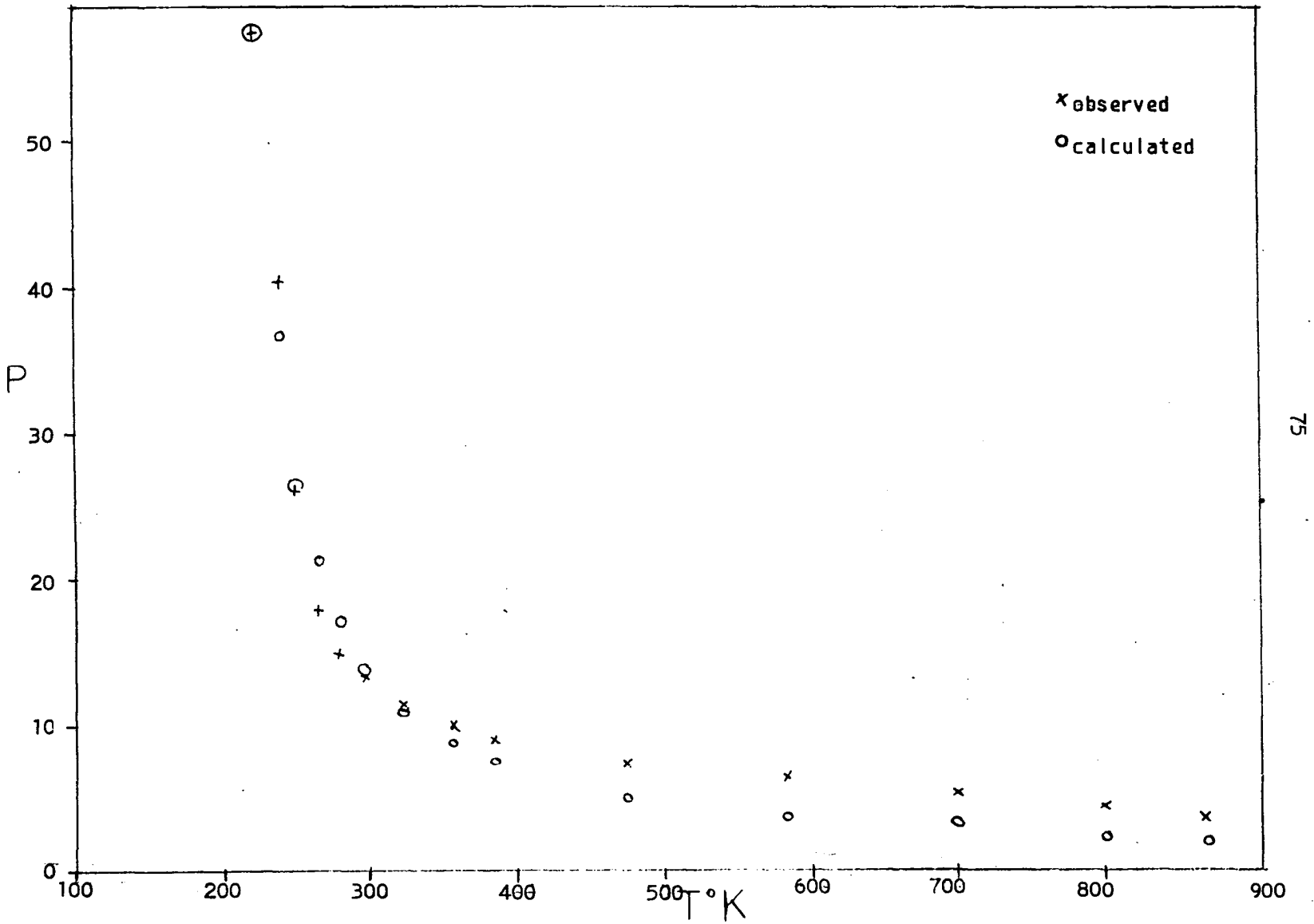

Fig. 25.—Comparison of Empirical Values With Experimental Values – KBr

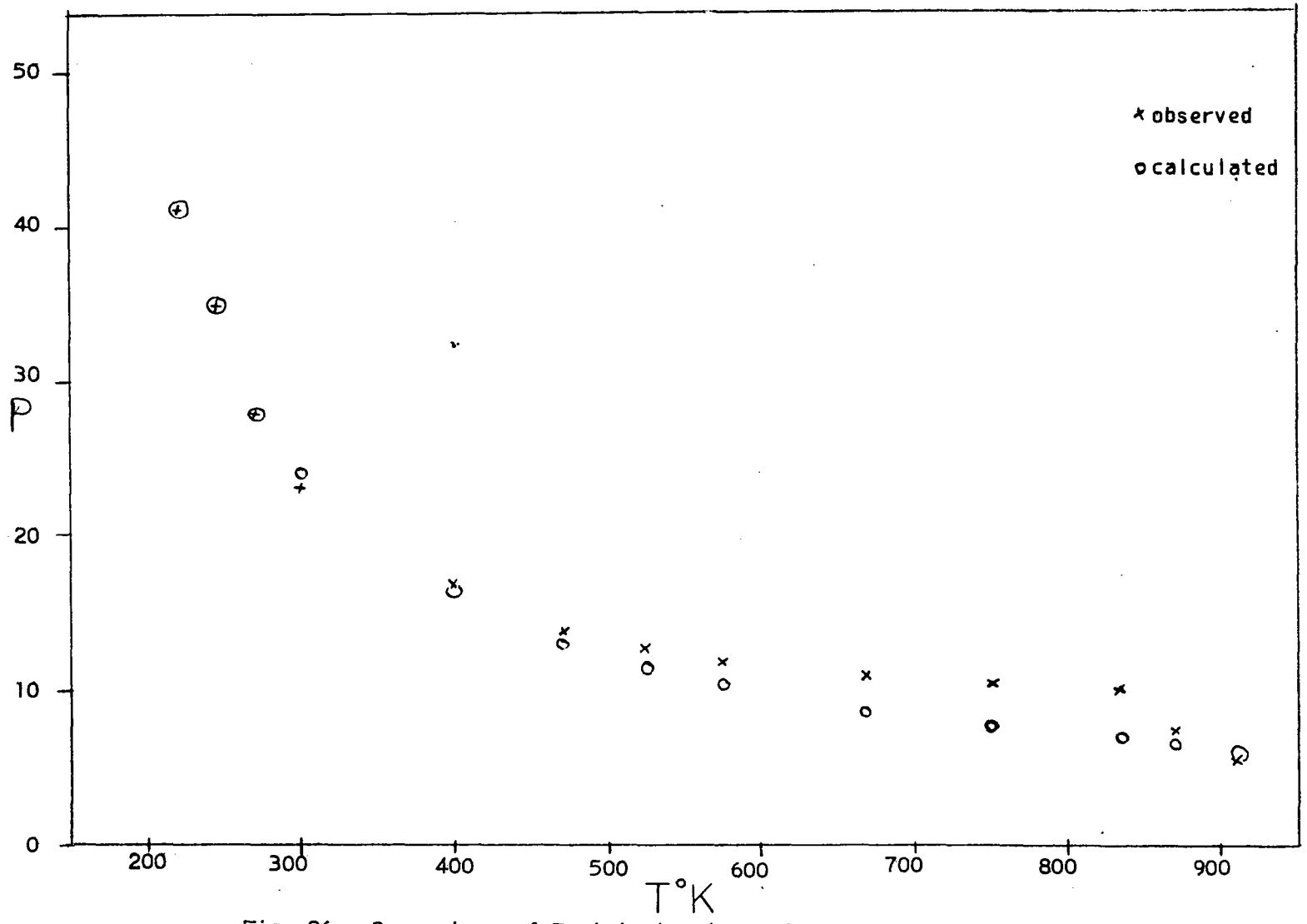

Fig. 26.--Comparison of Empirical Values With Experimental Values - KC1

where A and B are constants, B is identified the heat of solution or nucleation energy.

We shall now attempt to combine this idea with the theory set up by Koehler. Koehler defines a screening constant K such that

$$K^2 = \frac{8\pi Ne^2c}{\epsilon kT} \quad ,$$

and then proceeds to show that $1/K$ is proportional to the effective radius of the charge cloud. This radius was denoted earlier by the symbol r*. Hence $r^* \propto \sqrt{\frac{T}{c}}$, where T is the absolute temperature and c is the average concentration of dissolved divalent impurities within the crystal. If the divalent impurity concentration varies, so also must the radius of the dislocation.

Next we correlate the above information with what is already known about variation of scattering power with change in the effective radius of the charge cloud. To do this we try several plausible functions for $\rho(r)$ the radial distrubtion function and observe the form of the resultant scattering power. If we first assume $\rho(r)$ is of the form

$$\rho(r) = A'e^{-r/r^*} \tag{57}$$

where r* is the effective radius of the charge cloud, and A' is a constant, we obtain an expression in which the scattering power is a function of $\frac{1}{r^{*2}}$. If we next try $\rho(r) = \frac{B}{r}$, we again obtain a function of $\frac{1}{r^{*2}}$ for P. It therefore appears that the scattering power must somehow change as $\frac{1}{r^{*2}}$, and we shall presently check a formula of this type with the experimental data.

The scattering power in the region below the saturation peak

should then be of the form

$$P \propto \frac{1}{r^{*2}} \propto \frac{c}{T} \propto \frac{A n_e^{-B/kT}}{T} \qquad (58)$$

Formula (58) indicates that as the concentration decreases, the effective radius r* should increase, and hence the scattering power should fall off toward lower temperatures. At the saturation temperature the core of the dislocation line has an impurity atom at each lattice site. The increased scattering at saturation then may be thought of as being caused by a cylindrical volume of impurity atoms. As the temperature is decreased below saturation, the impurity precipitates into a new phase and takes the form of small spherical globules rather than the larger cylindrical region found at, and above, saturation. Plint and Sibley (24) calculate, with the aid of scattering formulae given by van de Hulst (29), that the scattering power should decrease at least by an order of magnitude when the cylindrical region is replaced by groups of small spheres. From this point of view the decrease in scattering power at the low temperature side of saturation seems quite plausible. This drop-off is observed experimentally as may be seen in Figure 6.

The experimental data fits quite nicely to formula (58) indicating possibly that precipitation of impurities is one of the few processes that can occur at the temperatures in question.

In Formula (58) the values of B for NaCl, KCl, and KBr were found to be 0.057 ev, 0.045 ev, and 0.053 ev respectively. These values for B must somehow be related to the work of nucleation. The work of nucleation and the stable nucleus size both depend upon the degree of saturation and decrease with increased degree of saturation. These

values for work of nucleation are not known theoretically. However, the energies listed above correspond to precipitation free energy changes of the order of 10^6 joules/Kg-mol and are comparable in size with the molar heats of fusion for water and hydrogen. Thus the identification of the decreasing scattering power with decreasing temperature below the peak with the onset of precipitation seems plausible.

It will be noticed that the theoretical form for the scattering power on the low temperature side of the peak is quite different from the empirically fitted forms 53, 54, 55. However, both forms are polynomials and thus can always be fitted approximately to the data. The theoretical form has some physical basis and is to be preferred over the empirical form.

In the region above the saturation peak, we will assume that the impurity ion concentration has reached the constant value c_0. In this range the impurity ions move away from the core of the dislocation, thereby causing the radius of the dislocation line to increase. The scattering power should then have the form:

$$P \propto \frac{1}{r^{*2}} \propto \frac{1}{T} \qquad (59)$$

If one attempts to fit formula (59) to the experimental data, one finds that the experimental curve and the calculated curve have the same general shape but are slightly displaced, the calculated values being larger than the experimental values. This discrepancy may arise because we have assumed that only the changes in r^* are important. The theory shows that the screening radius r^* is approximately proportional to $1/\kappa$ but other factors besides changes in r^* must be considered, among these is

the possibility of changes in n*. The average excess defect concentration in the cloud must be proportional to the charge on the dislocation line. Since this charge decreases with temperature (23), the excess defect concentration will also decrease and produce a decrease in the scattering power of the cloud. Such decrease would be over and above that caused by changes in r* and could, therefore, account for the difference between the experimental curve and the simple theoretical curve. Figure 27 shows both the low and high temperature results of this comparison for KCl.

In the foregoing discussion the change in scattering power was considered as being caused by the change in the divalent ion concentration at low temperature and to the increase in radius of the dislocation line caused by migration of impurities away from the core at high temperature. Above 600° K the concentration of intrinsic Schottky vacancies approaches that of the extrinsic vacancies and one would, in general, expect that the effects of impurities would be overshadowed somewhat by the effects produced by these intrinsic vacancies. These effects are perhaps observed in the deviations of the calculated scattering power from that observed experimentally at the high temperatures.

On the high temperature side of the peak, the scattering power decreases because the effective radius of the dislocation is increasing. This means that the defects in the neighborhood of the core are moving away from the dislocation, thereby reducing the value of $\overline{n^*}$, which is a measure of the difference in the average concentration of defects in the bad region as compared to the good crystal. Since $P \propto \overline{n^{*2}}$, one can calculate the changes taking place in terms of $\overline{n^*}$ as the core drops below the saturation point. For KCl:

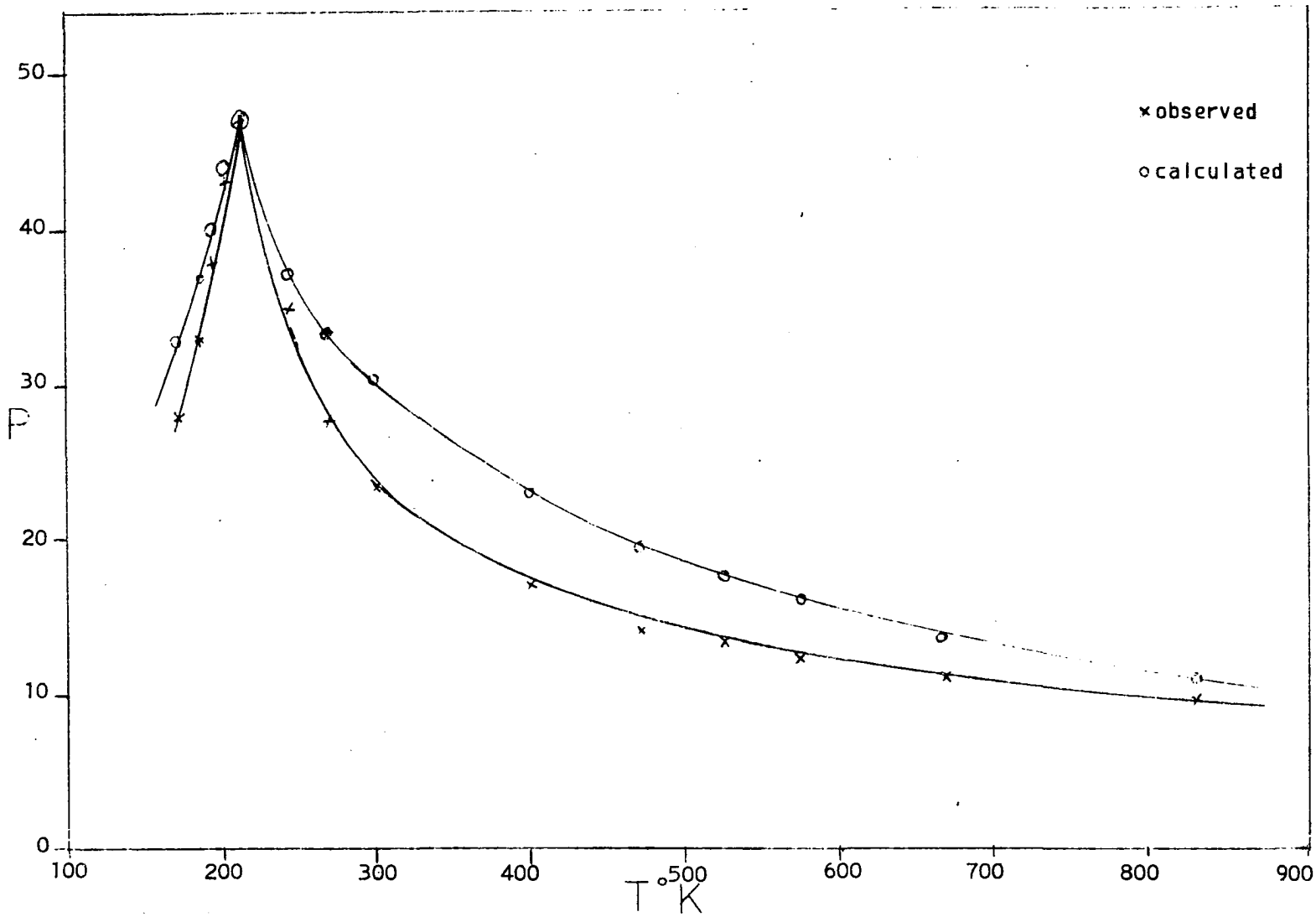

Fig. 27.—Comparison of Theoretical Values With Experimental Values – KCl

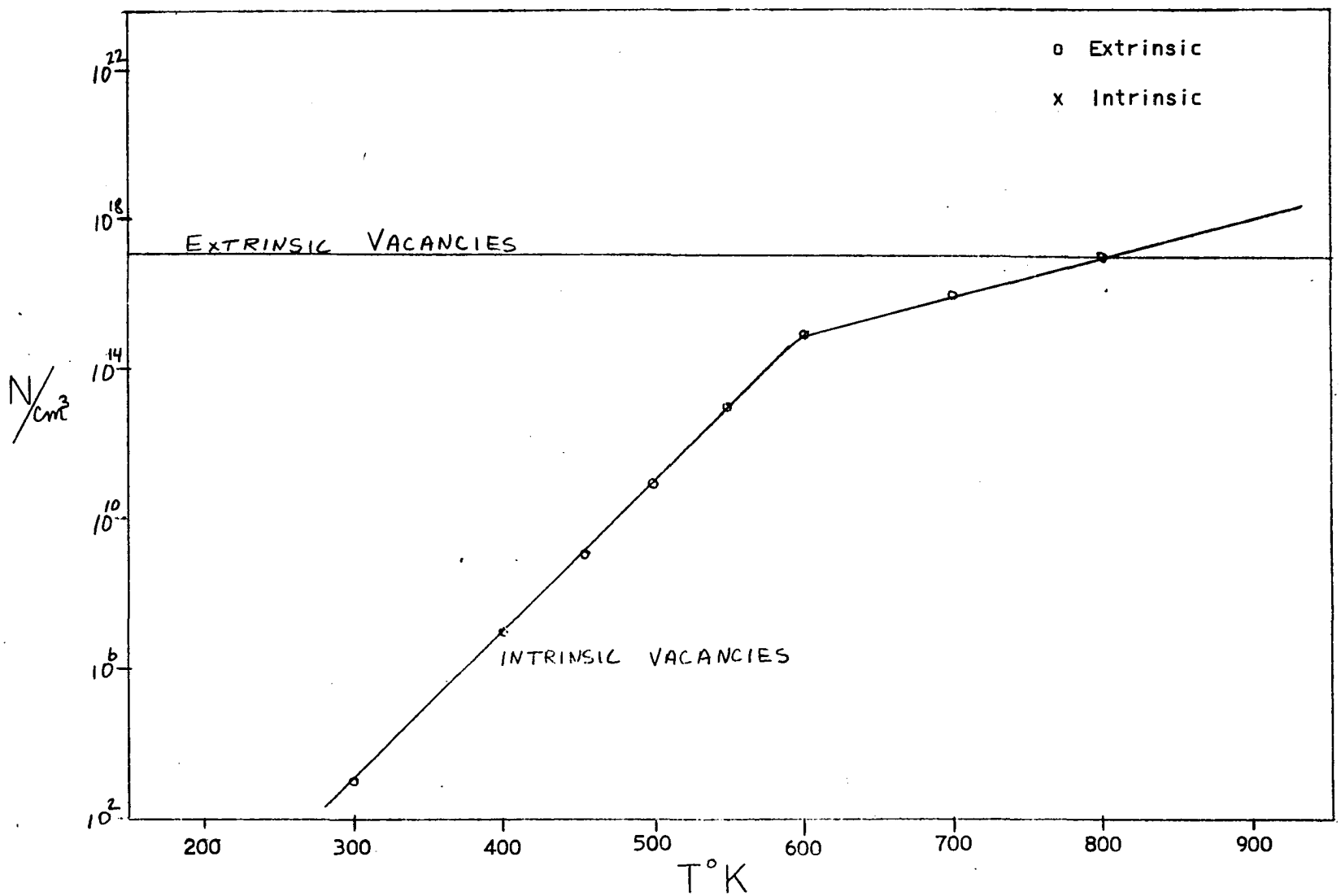

Fig. 28.--Comparison of Intrinsic Vacancy Concentration With Extrinsic Vacancy Concentration - KCl

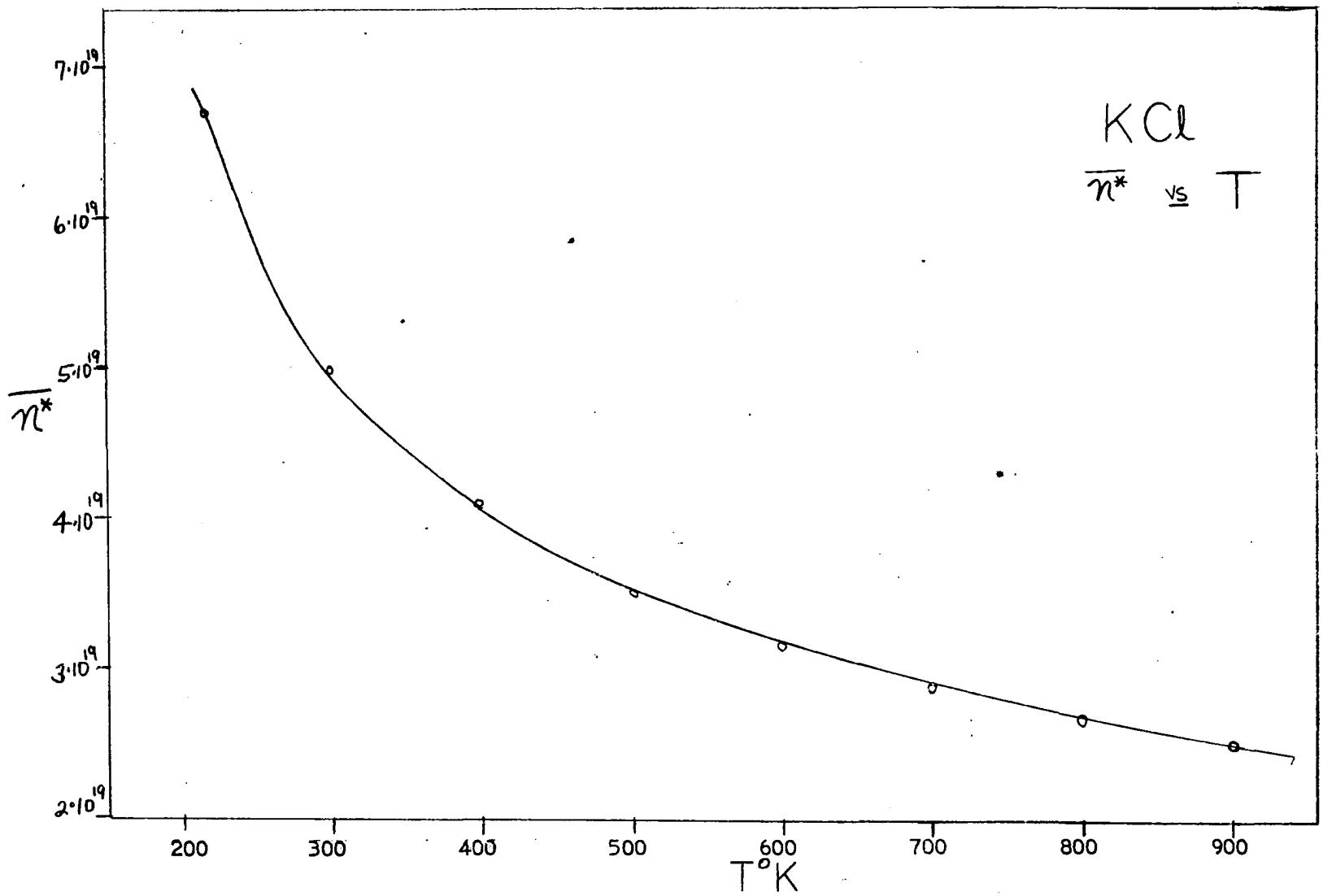

Fig. 29.--Variation of $\overline{n^*}$ With Temperature

$$\overline{n^*} \propto \left(\frac{1}{T - T_0}\right)^{\frac{1}{2}} \qquad (60)$$

Now it is known with a fair degree of accuracy that for Harshaw KCl at room temperature the value of $\overline{n^*}$ is approximately $5 \times 10^{19}/cm^3$. This result allows one to calculate the constants in Equation (60). The variation of $\overline{n^*}$ with temperature is shown in Figure 29. According to this theory, the value of $\overline{n^*}$ at saturation is $7 \times 10^{19}/cm^3$. The values of $\overline{n^*}$ indicate that an average has been performed over the entire dislocation, including the charge cloud. Of more interest perhaps, would be the average defect concentration at the core. For the two types of radial distribution function discussed here, one can calculate the average defect concentration at the core during saturation. If one assumes a radial distribution function of the type $\rho(r) = Ae^{-r/r^*}$, one obtains the value $n^* \simeq 10^{20}/cm^3$, and $n \simeq 3.5 \times 10^{21}/cm^3$ if one assumes $\rho(r) = \frac{B}{r}$ for the radial distribution function. These values seem quite plausible since there are in the neighborhood of 10^{21}–10^{22} lattice sites per cm^3 available, and at saturation each site should be filled with an impurity atom.

Fast Quench Treatment

The variation of scattering power with temperature of quench for KCl, KBr, and NaCl may be seen in Figure 21. There are two distinct ranges present. In the first range the scattering power decreases slightly with quench temperature. The slope of Ln P versus 1000/T is approximately the same as that obtained for equilibrium treatment, indicating that perhaps the processes responsible for the variation of scattering power are quite similar for the two treatments. The second

range starts at about 452° C, 490° C, and 560° C for KBr, KCl, and NaCl respectively. Above these temperatures the scattering power increases quite rapidly with temperature. This increase in scattering power has been discussed previously by Plint and Sibley (24), and only a brief sketch will be attempted here.

Etch pit counts on KCl and NaCl show a marked increase in dislocation density in the fast quench crystals over the annealed ones. In some cases an increase of as much as an order of magnitude was observed. This vastly increased dislocation count undoubtedly will cause an increase in the scattering power. Plint and Sibley observe that the scattering power for quenched Harshaw KCl increases sharply at temperatures near 300° C. This increase continues until the temperature reaches a value near the break in the conductivity curve, and drops quite sharply to a very low value. A similar result was obtained in this experiment, with one exception. The sharp drop in scattering power observed by Sibley was not observed. Instead, the scattering power increased sharply at a point near the break in the conductivity curve and continues to increase up to temperatures quite near the melting point of the crystal. However, it should be mentioned that Sibley's crystals were treated quite differently from those used in this investigation. They were less pure than the crystals used here, and the rate of quench was considerably slower.

When one attempts to compare the equilibrium scattering with the scattering from quenched crystals, one immediately sees that they are not at all the same. Whereas the equilibrium scattering decreases slowly with increase in temperature and then drops sharply at high temperatures, the fast quench scattering decreases slowly at first and then rises quite

sharply at high temperatures.

Etch pit counts show that the annealed crystals have a slightly larger dislocation count than the "as grown" crystals. Since the scattering power for the annealed crystals continues to decrease slowly, the greater dislocation count must be associated with dislocation loops at the surface which would not scatter light appreciably. Extensive formation of dislocation loops has been observed by Gilman and Johnston (8) for LiF; and although this material is much softer than the alkali halides under investigation, it is reasonable to expect similar behavior for all alkali halides. There were more dislocations in the fast quenched crystals than in the "as grown" crystals by a factor 10. Some experimenters claim that the quenching seals in the high temperature configuration. This is clearly not true, as a comparison of the scattering power for the quenched and annealed crystals indicates. Another point in favor of the statement that the equilibrium treatment is not the same as the quench treatment, is the question of reversibility of the scattering data. For the annealed crystals the scattering power data was completely reversible, while it was irreversible for the quench treated crystals. The scattering power observed for quenched crystals depended only on the highest quench temperature. A similar result was obtained by Sibley.

Suggestions For Further Work

There is a large group of experiments that should be done in connection with the investigation of defects in ionic crystals by the method of light scattering. The following investigations are recommended:

(1) An accurate measurement of the impurity content of the crystals is very important in order to further exploit

the possible method of measuring the energy of formation of positive ion vacancies in alkali halide crystals described in this thesis.

(2) Scattering work of the type discussed in this thesis should be done for samples with several different impurity concentrations.

(3) Complete angular dependence of the equilibrium scattering at high temperatures should be performed in order to detect any changes in the shape of the bad regions at high temperature.

(4) The temperature dependence of light scattering from crystals strained in a manner similar to that done by Sproull should be measured.

(5) An investigation of small angle scattering might give information concerning the shape and size of precipitates present at low temperatures below the observed peaks.

The above list is a very small portion of the experiments that need to be done if one is to continue to progress in the use of light scattering as a tool to investigate defects in ionic crystals.

REFERENCES

1. Charles Kittel, Introduction to Solid State Physics, 2nd ed. (New York: John Wiley & Sons, inc., 1956), p. 1.

2. Frederick Seitz, The Modern Theory of Solids (New York: McGraw Hill Book Co., Inc., 1940), p. 460.

3. A. H. Cottrell, Dislocations and Plastic Flow in Crystals (London: Oxford Press, 1956), p. 2.

4. A. H. Cottrell, Dislocations and Plastic Flow in Crystals (London: Oxford Press, 1956), p. 2.

5. F. C. Frank, Physica, 15 (1949), p. 131.

6. A. B. Lidiard, Handbuch der Physik, ed. by S. Flügge, (Berlin: Springer-Verlag, 1957), XX, p. 259.

7. S. Amelinckx, Acta Met. 2 (1954), 6, p. 848.

8. W. G. Johnston and J. S. Gilman, J. App. Phys. 30 (1959), p. 129.

9. O. Theimer and C. A. Plint, Ann. Phys. 3 (1958), p. 408.

10. S. Bhagavantam, Scattering of Light and the Raman Effect (Waltair: Andra University, 1940).

11. C. A. Plint, O. Theimer, and W. A. Sibley, Ann. Phys. 5 (1958), p. 342.

12. O. Theimer, C. A. Plint, and W. A. Sibley, Ann. Phys. 9 (1960), p. 475.

13. Lucienne Taurel and S. P. F. Humphreys-Owen, Proc. Phys. Soc. 75 (1960), p. 473.

14. W. K. H. Panofsky and Melba Phillips, Classical Electricity and Magnetism (Mass.: Addison-Wesley Pub. Co., Inc., 1962), p. 257.

15. D. M. Lester, Thesis, University of Oklahoma (1960).

16. Jerry C. Powell, Thesis, University of Oklahoma (1959).

17. D. Theimer and J. Canfield, J. App. Phys. 30 (1961), 2, p. 570.

18. K. Lehovec, J. Chem. Phys. 21 (1953), p. 1123.

19. J. D. Eshelby, C. W. A. Newey, P. L. Pratt, and A. B. Lidiard, Phil. Mag. 3 (1958), p. 75.

20. W. Metag, Z. Physik, 78 (1932), p. 363.

21. W. Burgsmuller, Z. Physik, 80 (1933), p. 299.

22. R. L. Sproull, Phil. Mag. 6 (1961), p. 1.

23. J. S. Koehler, D. Langreth, and B. von Turkovich, Phys. Rev. 128 (1962), 2, p. 573-580.

24. C. A. Plint and W. A. Sibley, J. App. Phys. 33 (1962), p. 3167.

25. M. Sakamoto and S. Kobayashi, J. Proc. Phys. Soc. Japan 13 (1958), p. 800.

26. W. A. Sibley, Dissertation, University of Oklahoma (1960).

27. W. A. Sibley, Private Communication.

28. N. F. Mott and M. J. Littleton, Trans. Faraday Soc. 34 (1938), p. 485.

29. H. C. van de Hulst, Light Scattering by Small Particles (New York: John Wiley & Sons, Inc., 1957), p. 99.

BIBLIOGRAPHY

Amelinckx, S., Acta Met. 2 (1954), 6, p. 848.

Bhagavantam, S., Scattering of Light and the Raman Effect (Waltair: Andra University, 1940).

Burgsmuller, W., Z. Physik 80 (1933), p. 299.

Cottrell, A. H., Dislocations and Plastic Flow in Crystals (London: Oxford Press, 1956).

Eshelby, J. D., C. W. A. Newey, P. L. Pratt, and A. B. Lidiard, Phil. Mag. 3 (1958), p. 75.

Frank, F. C., Physica 15 (1949), p. 131.

Johnston, W. G., and J. S. Gilman, J. App. Phys. 30 (1959), p. 129.

Kittel, Charles, Introduction to Solid State Physics, 2nd ed. (New York: John Wiley & Sons, Inc., 1956), p. 1.

Koehler, J. S., D. Langreth, and B. von Turkovich, Phys. Rev. 128 (1962), 2, p. 573-580.

Lehovec, K., J. Chem. Phys. 21 (1953), p. 1123.

Lester, D. M., Thesis, University of Oklahoma (1960).

Lidiard, A. B., Handbuch der Physik, ed. by S. Flügge, (Berlin: Springer-Verlag, 1957), XX, p. 259.

Metag, W., Z. Physik 78 (1932), p. 363.

Mott, N. F., and M. J. Littleton, Trans. Faraday Soc. 34 (1938), p. 485.

Panofsky, W. K. H. and Melba Phillips, Classical Electricity and Magnetism (Mass.: Addison-Wesley Pub. Co., Inc., 1962), p. 257.

Plint, C. A., O. Theimer, and W. A. Sibley, Ann. Phys. 5 (1958), p. 342.

Plint, C. A. and W. A. Sibley, J. App. Phys. 33 (1962), p. 3167.

Powell, Jerry C., Thesis, University of Oklahoma (1959).

Sakamoto, M. and S. Kobayashi, J. Proc. Phys. Soc. Japan 13 (1958), p. 800.

Seitz, Frederick, The Modern Theory of Solids (New York: McGraw Hill Book Co., Inc., 1940), p. 460.

Sibley, W. A., Dissertation, University of Oklahoma (1960).

Sproull, R. L., Phil. Mag. 6 (1961), p. 1.

Taurel, Lucienne and S. P. F. Humphreys-Owen, Proc. Phys. Soc. 75 (1960), p. 473.

Theimer, O. and C. A. Plint, Ann. Phys. 3 (1958), p. 408.

Theimer, O., C. A. Plint, and W. A. Sibley, Ann. Phys. 9 (1960), p. 475.

Theimer, O. and J. Canfield, J. App. Phys. 30 (1961), 2, p. 570.

van de Hulst, J. C., Light Scattering by Small Particles (New York: John Wiley, & Sons, Inc., 1957), p. 99.